International Geology Review, Vol. 45, 2003, p. XXX–XXX.
Copyright © 2003 by V. H. Winston & Son, Inc. All rights reserved.

Geochemistry and Petrogenesis of Cenozoic Andesite-Dacite Associations from the Hoh Xil Region, Tibetan Plateau

LAI SHAOCONG,[1] LIU CHIYANG,

Ministry of Education Key Laboratory of Continental Dynamics, Department of Geology, Northwest University, Xi'an 710069, China

AND YI HAISHENG

Chengdu University of Technology, Chengdu 610059, China

Abstract

Volcanic units with ages in the range 4.27–44.60 Ma in the Zhentouya area south to Ulan Ul Lake, Hoh Xil region, are mainly lava, predominantly dacite in composition, together with lesser amounts of andesite. The high-potassium calc-alkaline dacite series is characterized by enriched LIL elements such as Rb, Ba, Th, U, and K, and depleted HFSE such as Ti, Nb, Ta, and Sr, whereas the andesite series containing high-potassium calc-alkaline and shoshonitic components is enriched in the LIL elements Cs, Rb, Ba, Th, U, and Sr, and depleted in the HFSE Ti, Nb, and Ta. La/Sm-La and Zr/Sm-Zr discrimination diagrams indicate that both the dacite and the andesite series, with their contrasting evolutionary trends, were generated from partial melting of the continental crust rather than by fractional crystallization of a primary basaltic magma derived from the mantle.

Nd, Sr, and Pb isotopic compositions of the dacite (radiogenic $^{87}Sr/^{86}Sr$ = 0.709227–0.709578, $^{208}Pb/^{204}Pb$ = 39.1356–39.2622, $^{207}Pb/^{204}Pb$ = 15.6675–15.7063, $^{206}Pb/^{204}Pb$ = 18.7635–18.7970 and nonradiogenic $^{143}Nd/^{144}Nd$ = 0.512287–0.512591, ε_{Nd} = –0.92 to –6.85) provide evidence that crustal anatexis in the Tibetan Plateau played an important role in petrogenesis of the dacite series. Moreover, the presence of granulite xenoliths in the dacite series places P-T constraints on the magma source at a temperature range of 780–820°C and pressure of 0.86 GPa (equal to a depth of 28 km). Combined with P-T conditions inferred from the granulite-facies xenoliths, the geochemistry of the dacite and the isotopic signature of crustal anatexis suggest that partial melting of the middle part of thickened Tibetan crust could have produced the primary dacite magma series.

The andesite, to some degree, shows an adakitic compositional signature involving high Sr >1000 ppm, Sr/Y ratios >50, and low Yb contents <2 ppm. Evidently plagioclase broke down in the andesitic magma source region under the P-T conditions of partial melting. Compared with the dacite series, it appears that partial melting of the lower part of the thickened, eclogite-facies Tibetan crust was responsible for generation of the andesitic magma.

Introduction

OVER THE PAST 50 million years, collision between India and Eurasia has produced the highest, most extensive plateau on Earth today, and the greatest present-day topographic relief. India has moved northward with respect to Asia at a substantial rate, apparently accommodated by internal deformation of India and Asia; seismic data indicate that the crust is twice normal thickness (75 km) (Molnar, 1988). The Tibetan Plateau has a great significance for the study of the mechanics of mountain belts (England and Houseman, 1988, 1989). The present elevation and extensional deformation of the plateau are generally regarded as a response to the convective removal of the lower portion of thickened Asian lithosphere (Platt and England, 1994). This removal is also thought to be responsible for E-W extension that has taken place during the India-Asia collision (Coleman and Hodges, 1995). Despite numerous studies of the region, processes responsible for formation of the plateau and the surrounding mountain ranges are still controversial. Three hypotheses (as summarized by Miller et al., 1999) have been suggested to explain the crust thickening and the elevation of Tibet. In the first, the entire Tibetan Plateau is underthrust by the Indian lithosphere (Argand, 1924; Powell and Conaghan, 1973; Ni and

[1]Corresponding author; email: shaocong@pub.xaonline.com

Baranzagi, 1984). In the second, thickening results from inflow of material from India (Zhao and Morgan, 1987). In the third, the crust of Tibet is interpreted as having been thickened by shortening (Dewey and Burke, 1973).

Cenozoic volcanic rock associations that are widely distributed in the Tibetan Plateau can contribute to our understanding of the uplift mechanism, formation processes, and development of the plateau. They provide information on past tectonic environments as an aid to the paleo-tectonic reconstruction of the plateau. Their geochemical and isotopic signatures provide a foundation to understand the magma source region characteristics, mantle/crust interaction, and continental collision processes. Such extrusive rocks have been studied for a long time in order to provide constraints on the uplift mechanism of the Tibetan Plateau (Ugo, 1990; Arnaud et al., 1992; Turner et al., 1996; Deng, 1998; Deng and Sun, 1998, 1999; Liu, 1998; Chi et al., 1999; Lai, 1999; Miller et al., 1999; Wang et al., 1999). Up to now, three volcanic series have been identified: ultrapotassic, shoshonitic, and high-potassium calc-alkaline. Petrologic, geochemical, isotopic, and genetic features of the ultrapotassic and shoshonitic volcanic rock series have been studied (Ugo, 1990; Arnaud et al., 1992; Turner et al., 1996; Deng, 1998; Liu, 1998; Deng and Sun, 1998, 1999; Chi et al., 1999; Lai, 1999; Miller et al., 1999; Wang et al., 1999).

The Tibetan Plateau has a crust as thick as 70–75 km (Wortel et al., 1992). What happened in the middle-lower crust of the plateau during the Cenozoic period? Do geological conditions in the middle-lower crust of the plateau favor generation of intermediate and silicic volcanic rocks? If so, what kinds of magma were generated? Available data suggest that processes responsible for generation of the intermediate-silicic volcanic rock association in the Hoh Xil and north Qiangtang areas are still unclear (Lai and Liu, 2001). This paper documents the presence of Cenozoic andesite-dacite associations in the Zhentouya area, Hoh Xil region, and presents detailed geochemical compositional and Sr-Nd-Pb isotopic data for these rocks. In addition, granulite xenoliths contained mainly in the dacite are described in detail. The main objective is to better understand the middle-lower crustal magmatic processes attending Cenozoic thickening of the Tibetan Plateau. We then discuss their source and origin, and propose a preliminary model for the generation of the intermediate-silicic crust-derived andesite-dacite associations in the Hoh Xil region.

General Geological Setting

Distributed from the Shishui River, via the Yudai Mountain, to the Yanshiping area in northern Tibet, Cenozoic volcanic rocks crop out as 50- to 200-meter-thick lava sheets and long flows. The rocks overlying the Neogene Suona Lake group (N_{1s}) and the Jurassic Yanshiping group (J_{2ys}) belong to the Shipingding group (N_{1sh}) defined by the north Qiangtang stratigraphic classification (Zhang and Zheng, 1994). The Cenozoic volcanic series is characterized by overflow volcanics with minor pyroclastic rocks, representing a subaerial eruption of the central type. Some subvolcanic rocks generated in the volcanic conduit or nearby the crater also support this type of eruption (Fig. 1).

This study focuses on the volcanic rocks exposed in the Zhentouya area, south to the Ulan Ul Lake area, Hoh Xil region (Fig. 1). The main rock type is andesite and dacite, belonging to a typical intermediate-silicic magma series. Basalts have not been reported in this area. According to field observation, the volcanic rocks were generated in two eruption cycles, between which there is a separation of a 20 to 30 meter-wide layer of volcanic breccia (Fig. 2). The first eruption cycle is dominated by andesite, and the second by dacite. Granulite xenoliths have been identified from both andesitic series and dacitic series, but are mainly contained in the latter (Fig. 2). The volcanic rocks discordantly overlie the Tertiary Tuotuo River group (Et) (Fig. 2), so the age of the volcanic rocks in the area lies between the Tertiary and the Quaternary. Isotopic ages determined by the K-Ar method range from 4.27 Ma to 44.66 Ma (Zhang and Zheng, 1994; Deng, 1998), which fall into the age range from the above stratigraphical constraint. Therefore, the major part of the volcanic rocks in the Zhentouya area was probably formed during the period from the Late Paleogene to the Neogene.

Sample and Analytical Techniques

All samples were examined first by microscopice study. Weathered and altered parts of the samples were carefully removed and the unaltered specimens were cut into small chips with a diamond saw. The surface of the small chips was carefully cleaned in deionized water, then dried and further hand

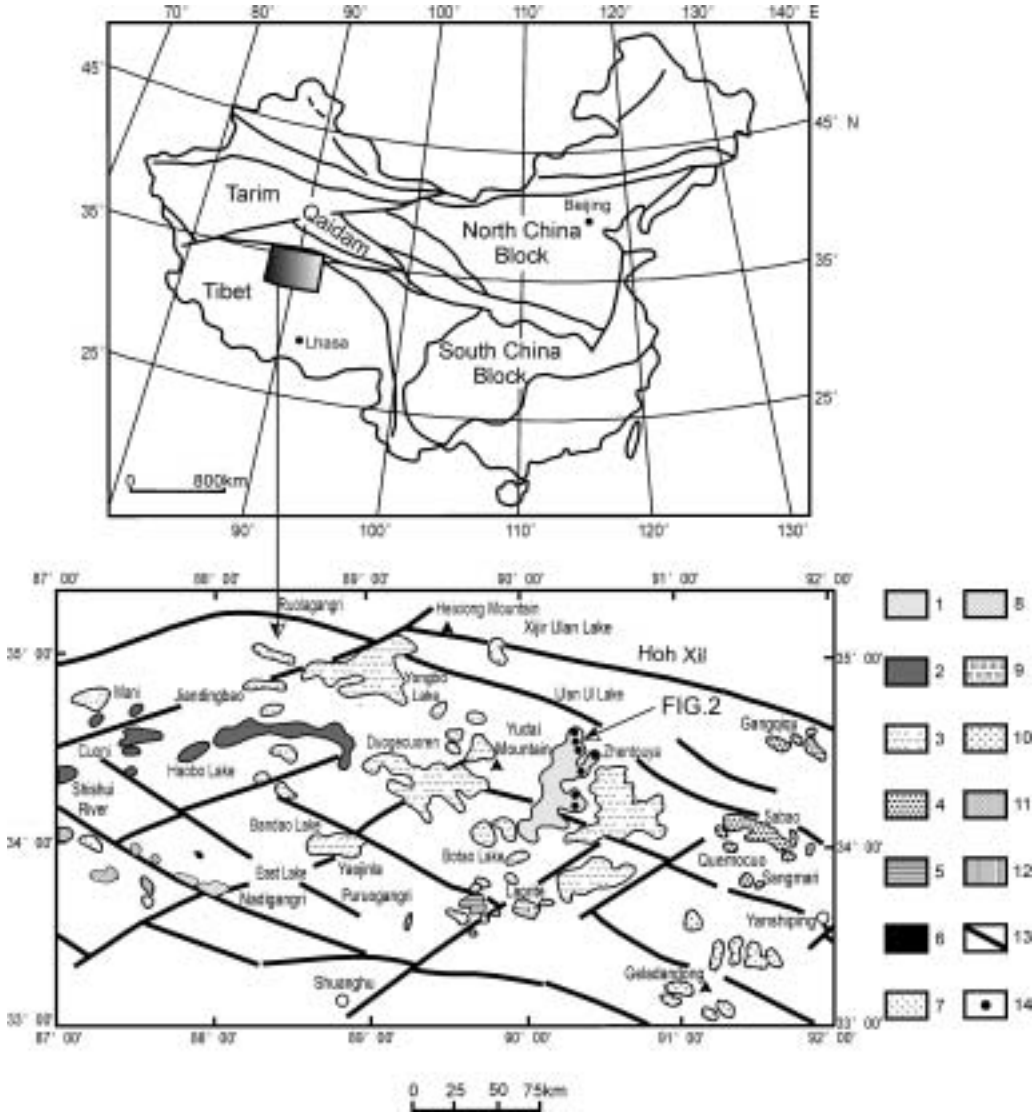

FIG. 1. Regional distribution of Mesozoic–Cenozoic magma rocks in the north Tibet area. Legend: 1 = Late Paleogene to Neogene andesite and dacite; 2 = Neogene adakitic rocks (Lai et al., 2003); 3 = Neogene ultrapotassic and shoshonitic volcanic rocks; 4 = Paleogene quartz-syenite porphyry; 5 = Paleogene quartz-monzodiorite porphyry; 6 = Paleogene basaltic-trachyandesite porphyry; 7 = Cretaceous volcanic rocks; 8 = Late Cretaceous rhyolite porphyry; 9 = Late Cretaceous adamellite porphyry; 10 = Late Cretaceous adamellite; 11 = Late Cretaceous granodiorite; 12 = hypabyssal intrusive; 13 = fault; 14 = sampling locality.

crushed. Powder of each sample was made from 50 to 100 g splits with a tungsten carbide shatterbox at the Key Laboratory of Continental Dynamics, Northwest University, Xi'an.

Major elements were analyzed by means of wet chemistry at the Institute of Geochemistry, Chinese Academy of Sciences. Analyses of trace elements, including rare earth elements (REE), was performed by a Finnigan MAT ELEMENT magnetic sector inductively coupled plasma mass spectrometer at the Institute of Geochemistry, Chinese Academy of Sciences. PTFE screw-top bombs were used to serve

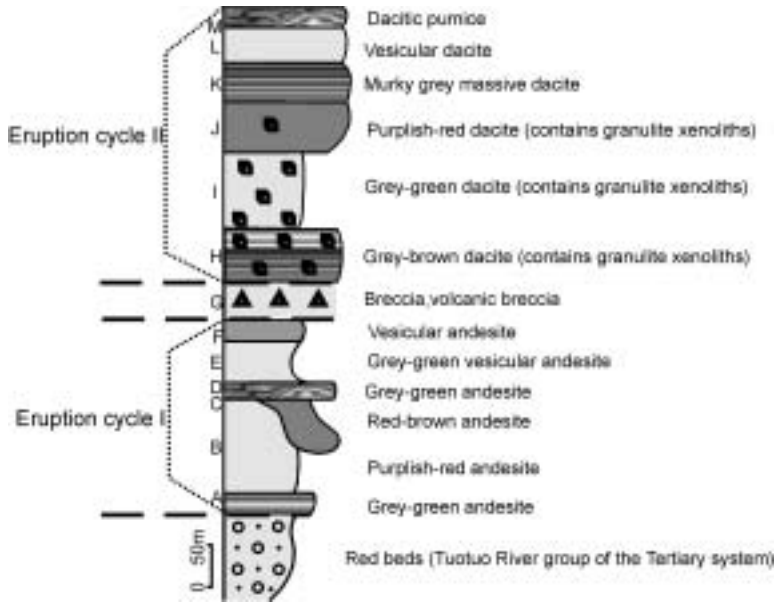

FIG. 2. Stratigraphic column for Late Paleogene to Neogene age andesite and dacite associations distributed in the Zhentouya area, Hoh Xil region.

sample dissolution. Analytical reagent-grade HF and HNO_3 were purified prior to use by sub-boiling distillation. The PTFE bombs were cleaned by 20% HNO_3 (v/v) and heated to 100°C for 1 hour in an oven. The procedure for the ICP-MS analysis is similar to that described by Qi et al (2000), and Qi and Gregoire (2000). Trace-element concentrations were drift corrected to those of standard BCR-1; analytical uncertainties are generally better than 5% for most elements.

Sr-Nd isotope ratios and contents were determined through isotope dilution techniques on a Finnigan MAT-261 multicollector mass spectrometer at the Chinese Academy of Geological Sciences. Nd isotopic ratios were measured in metal form, mass fractionation corrected to $^{146}Nd/^{144}Nd$ = 0.7219, and are reported relative to $^{143}Nd/^{144}Nd$ = 0.511125 for the J.M.Nd_2O_3 standard and $^{143}Nd/^{144}Nd$ = 0.512725 for the GBW04419 standard. Analytical uncertainty for $^{143}Nd/^{144}Nd$ measurements is $\pm 2\sigma$. Sr isotopic ratios were also measured in metal form, mass fractionation corrected to $^{88}Sr/^{86}Sr$ = 8.37521, and are reported in reference to $^{87}Sr/^{86}Sr$ = 0.71025 for the NBS987 $SrCO_3$ standard. The level of background contamination for Sm and Nd is $< 5 \times 10^{-11}$ g and for Rb and Sr $< 10^{-9} - 10^{-10}$ g.

For Pb analysis, 200 mg of rock powder was dissolved with bi-distilled hydrofluoric and perchloric acids in a clean Teflon bomb. Pb was separated from the silicate matrix employing HCl ion-exchange procedures. The Pb isotopes were measured on a Finnigan MAT-261 mass spectrometer in a static mode with Re single filaments and the silica-gel-phosphoric acid technique. Pb isotopic fractionation was corrected off-line with correction factors derived from NBS SRM987 standard measurements. The level of background contamination for Pb is $< 2 \times 10^{-10}$ g .

Petrology and Chemical Composition

The studied andesite is characterized by phenocrysts of plagioclase ± amphibole ± biotite. Pyroxene phenocrysts occur in some samples. The groundmass shows a fine-grained texture, with minor volcanic glass. Small amounts of apatite and magnetite are restricted to the groundmass. The andesite is slightly altered, with feldspars kaolinized, mafic minerals chloritized, and carbonates invading vacuoles and fractures. However, alteration is rather limited. Judged by the presence of vesicular and amygdaloidal structures, and aphyric and

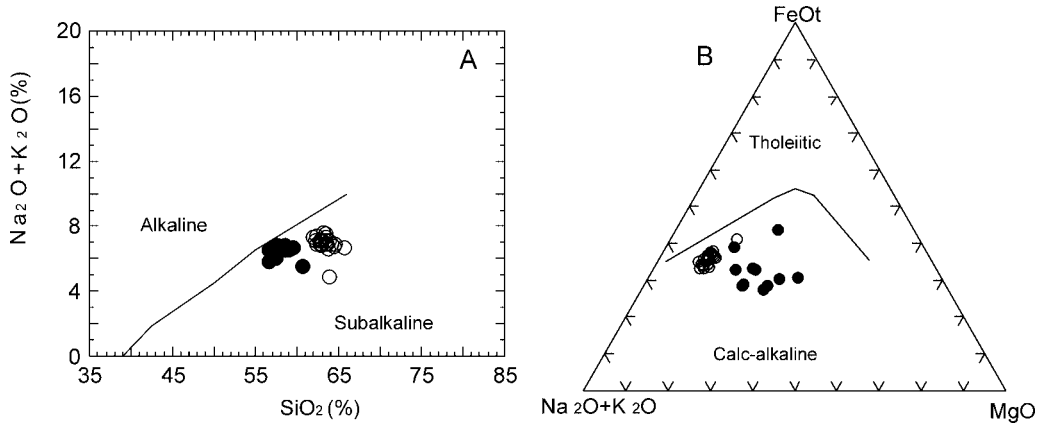

FIG. 3. SiO2–(K_2O + Na_2O) (A) and Alk-FeO-MgO (B) diagrams for the andesite (solid circles) and dacite (open circles) from Zhentouya area, Hoh Xil region.

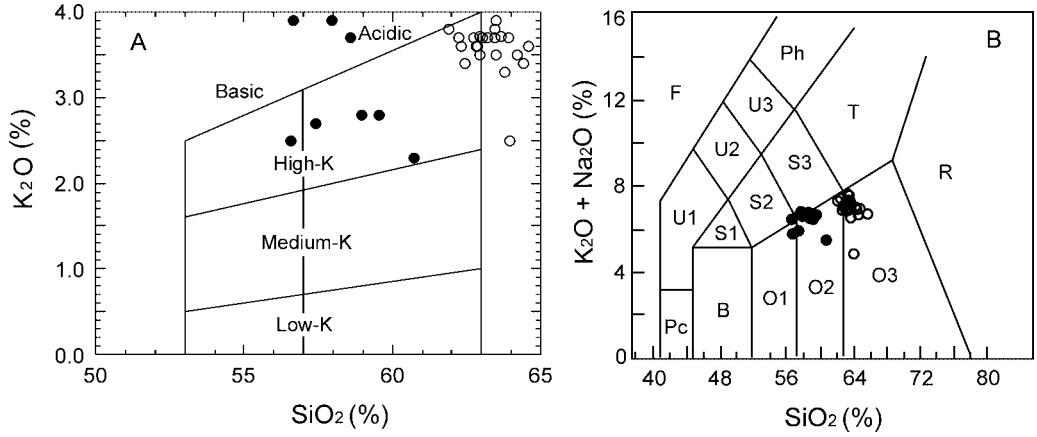

FIG. 4. SiO_2 versus K_2O diagram (A) and TAS classification schemes (B) (after Le Bas,1986) for the andesite (solid circles) and dacite (open circles) from the Zhentouya area, Hoh Xil region. Low-K = low-potassium calc-alkaline series; medium-K = medium-potassium calc-alkaline series; high-K = high-potassium calc-alkaline series; SHO = shoshonitic series; F = foidite; U1 = tephrite (Ol < 10%), basanite (Ol > 10%); U2 = phonotephrite; U3 = tephriphonolite; Ph = phonolite; S1 = trachybasalt; S2 = basaltic trachyandesite; S3 = trachyandesite; T = trachyte (*q* < 20%), trachydacite (*q* > 20); Pc = picrobasalt; B = basalt; O1 = basaltic andesite; O2 = andesite; O3 = dacite; R = rhyolite.

porphyro-aphanitic textures, the dacite is relatively fresh. The porphyro-aphanitic dacite in many samples contains phenocrysts of quartz, amphibole, biotite, and plagioclase. The groundmass with interlocking and hyalopilitic textures is fine-grained with abundant volcanic glass.

Major- and trace-element data of representative samples from the Zhentouya area, Hoh Xil region are given in Table 1. Two types of intermediate-silicic rocks were identified based solely on SiO_2 contents, namely andesite and dacite, with the latter dominant in volume over the former. Both andesite and dacite belong to the sub-alkaline series in the K_2O + Na_2O versus SiO_2 diagram (Fig. 3A) and show a calc-alkaline trend when plotted in the Alk-FeO-MgO diagram (Fig. 3B). In addition, the dacitic rocks plot as the high-potassium calc-alkaline series on an SiO_2 versus K_2O diagram (Fig. 4A), whereas the andesitic rocks are variable, from high-potassium calc-alkaline to shoshonite. In general, the TAS classification schemes (Fig. 4B) of Le Bas (1986) can be used to verify rock names. Thus the

TABLE 1. Major- (wt%) and Trace-Element (ppm) Analyses of Volcanic Rocks from the Zhentouya area, Hoh Xil region, Tibetan Plateau

Sample:	P22H5	P10H5	P14H6	P11H6	P11H7	P7H4	P16H6	P10H6	P13H3	P12H5	P3H6
Rock:	Andesite	Andesite	Andesite	Andesite	Andesite	Andesite	Andesite	Andesite	Andesite	Andesite	Andesite
SiO_2	56.59	56.65	57.43	57.53	57.68	57.94	58.56	58.59	58.98	59.57	60.74
TiO_2	0.65	0.75	0.50	0.85	0.87	0.82	0.97	0.77	0.52	0.55	0.50
Al_2O_3	15.31	14.21	14.21	14.75	14.21	13.78	15.09	15.31	17.50	17.06	17.66
Fe_2O_3	2.60	1.80	6.93	1.80	1.62	1.00	2.50	1.50	1.15	1.10	1.40
FeO	2.90	3.50	1.97	3.60	2.68	3.60	3.00	3.10	3.05	3.00	3.50
MnO	0.13	0.03	0.16	0.12	0.06	0.01	0.10	0.04	0.14	0.01	0.34
MgO	6.10	5.31	4.57	3.66	3.33	4.62	3.87	2.68	4.31	3.26	2.01
CaO	5.45	5.03	4.56	4.13	4.73	4.25	3.68	4.63	4.43	4.88	2.80
Na_2O	3.30	2.60	3.30	2.60	2.60	2.80	2.50	2.80	3.70	3.90	3.20
K_2O	2.50	3.90	2.70	4.20	4.20	3.90	4.30	3.70	2.80	2.80	2.30
P_2O_5	0.40	0.80	0.43	0.90	0.87	0.77	0.87	0.77	0.50	0.43	0.27
LOI	3.86	4.85	2.87	4.34	6.82	5.83	3.90	5.80	2.30	3.10	4.67
Total	99.79	99.43	99.63	99.48	99.67	99.32	99.34	99.69	99.38	99.66	99.39
Mg#[1]	0.685	0.668	0.493	0.577	0.609	0.672	0.589	0.539	0.674	0.616	0.449
Li	34.9	42.6	21.2	16.3	15.7	18.1	16.0	15.3	14.0	16.0	10.5
Be	1.19	3.32	2.12	3.60	3.44	4.19	3.75	3.24	1.97	2.12	1.90
Sc	17.8	15.3	12.8	16.2	16.1	15.0	16.5	14.3	13.1	13.0	14.4
V	115	97.2	86.3	113	110	107	113	104	92.7	87.9	95.8
Cr	416	298	215	363	366	348	368	303	223	221	155
Co	39.8	29.8	34.9	35.8	33.5	36.0	37.6	35.6	32.9	38.7	51.7
Ni	232	196	115	206	230	220	211	163	112	117	85.8
Cu	25.9	38.9	14.1	52.6	47.0	41.1	60.2	36.3	15.9	17.0	17.1
Zn	54.8	79.4	56.8	74.2	94.2	66.8	83.4	55.7	57.9	54.0	66.5
Ga	12.4	13.3	14.0	14.2	13.3	13.4	13.7	14.4	15.2	14.5	14.9
Ge	1.21	1.54	1.18	1.45	1.25	1.48	1.36	1.13	1.30	1.26	1.07
As	17.1	13.8	18.3	15.9	13.6	15.3	27.9	13.6	15.5	7.33	36.6
Rb	82.9	184	98.7	219	221	197	223	197	82.8	103	120
Sr	1165	1379	1653	1548	1546	1611	1555	1476	1629	1554	1003
Y	17.6	18.6	13.9	21.9	22.5	21.2	23.1	20.5	14.5	14.3	19.6
Zr	181	303	221	344	362	344	363	340	227	228	147
Nb	8.90	13.4	10.3	14.2	14.5	14.4	15.2	14.3	10.3	9.95	7.71
Mo	1.67	0.664	1.59	0.654	0.916	0.821	0.807	1.20	1.38	1.21	1.61
Cd	0.097	0.199	0.120	0.144	0.197	0.178	0.158	0.153	0.121	0.14	0.200
In	0.031	0.048	0.029	0.044	0.056	0.044	0.049	0.043	0.040	0.033	0.023
Sn	2.19	4.12	2.84	3.76	4.75	3.95	3.79	4.00	2.71	3.00	2.19
Sb	1.15	1.11	0.811	1.61	1.43	1.71	1.34	1.09	0.747	1.72	0.556
Cs	3.08	2.62	3.99	3.39	3.29	3.94	3.30	4.09	3.64	3.26	8.67
Ba	1481	1641	1437	1806	1807	1627	1789	1753	1552	1441	1530
Hf	5.02	8.97	6.48	10.3	10.6	9.88	10.6	9.55	6.53	6.49	4.49
Ta	0.547	0.770	0.573	0.877	1.08	0.786	0.852	0.803	0.614	0.567	0.587
W	62.3	28.4	107	62.5	64.8	78.9	73.3	112	102	131	87.0
Tl	0.307	0.822	0.566	0.795	0.771	0.860	0.837	0.618	0.432	0.441	0.706
Pb	30.1	27.5	32.0	27.7	29.3	28.2	28.1	28.5	30.8	25.3	32.0
Bi	0.102	0.067	0.402	0.109	0.171	0.049	0.075	0.103	0.194	0.193	0.042
Th	17.6	18.2	21.1	19.7	19.6	18.5	19.3	19.3	21.7	20.8	13.0
U	3.57	3.54	4.16	3.79	3.78	3.45	3.54	3.57	4.24	4.42	3.94
La	57.5	70.7	70.1	74.4	74.1	69.1	74.6	74.7	76.6	71.8	43.3
Ce	108	138	133	152	152	139	148	147	143	136	84.7
Pr	11.0	14.8	13.2	16.4	16.8	15.5	16.1	16.0	14.1	13.5	9.07
Nd	41.0	56.6	48.5	62.6	64.2	59.1	61.2	59.3	51.0	48.8	33.3
Sm	7.16	9.15	7.30	10.4	10.5	9.38	10.1	9.49	7.74	7.24	5.89
Eu	1.61	2.10	1.66	2.21	2.37	2.27	2.30	2.10	1.73	1.76	1.42
Gd	5.19	6.78	4.95	7.66	7.58	6.74	7.52	6.91	5.49	5.14	4.60
Tb	0.660	0.784	0.596	0.924	0.993	0.837	0.951	0.885	0.653	0.591	0.586
Dy	3.26	3.96	3.01	4.58	4.60	4.13	4.66	4.02	3.05	3.02	3.31
Ho	0.633	0.679	0.492	0.762	0.795	0.727	0.805	0.694	0.500	0.500	0.634
Er	1.70	1.85	1.31	2.12	2.18	1.88	2.25	1.92	1.47	1.35	1.82
Tm	0.221	0.231	0.167	0.270	0.275	0.263	0.300	0.244	0.172	0.162	0.230
Yb	1.49	1.59	1.08	1.82	1.81	1.68	1.95	1.70	1.22	1.16	1.52
Lu	0.229	0.263	0.167	0.267	0.258	0.243	0.302	0.241	0.180	0.157	0.230

Table continues

TABLE 1. *CONTINUED*

Sample:	P4H	P25H11	P25H6	P1H5	P3H1	P2H4	P8H	P1H2	P2H9	P1H1	P24H3	P25H8
Rock:	Dacite	Dacite	Dacite	Dacite	Dacite	Dacite	Dacite	Dacite	Dacite	Dacite	Dacite	Dacite
SiO_2	61.91	62.24	62.31	62.43	62.76	62.83	62.86	62.94	62.96	63.03	63.20	63.46
TiO_2	1.10	1.37	1.30	1.30	1.15	1.12	1.20	1.48	1.26	1.22	1.30	1.38
Al_2O_3	16.40	15.53	16.62	17.06	17.28	16.18	15.75	16.18	16.48	16.40	15.75	15.96
Fe_2O_3	2.21	2.20	1.90	1.45	1.40	1.85	1.65	1.40	1.50	1.45	2.73	1.80
FeO	3.19	2.50	3.50	3.25	3.20	3.51	3.55	3.20	3.50	3.49	2.27	2.90
MnO	0.06	0.14	0.13	0.12	0.08	0.10	0.05	0.12	0.07	0.13	0.08	0.12
MgO	1.55	1.26	1.62	1.52	1.61	1.66	1.51	1.52	1.82	1.54	1.61	1.42
CaO	4.09	4.88	3.41	2.61	2.97	3.08	3.85	3.08	2.76	3.14	3.13	3.28
Na_2O	3.50	3.40	3.30	4.00	3.20	3.50	3.30	3.40	3.31	3.40	3.90	3.50
K_2O	3.80	3.70	3.60	3.40	3.70	3.60	3.60	3.71	3.50	3.70	3.70	3.80
P_2O_5	0.73	0.93	0.83	0.90	0.83	0.87	0.73	0.90	0.76	1.13	0.83	0.84
LOI	0.90	1.42	1.02	1.50	1.20	1.05	1.30	1.30	1.30	1.19	1.33	1.03
Total	99.44	99.57	99.54	99.54	99.38	99.35	99.35	99.23	99.22	99.82	99.83	99.49
$Mg^{\#}$	0.363	0.347	0.374	0.394	0.413	0.383	0.369	0.400	0.422	0.386	0.389	0.377
Li	22.9	21.0	23.4	19.0	22.6	16.1	19.4	20.5	18.6	22.6	23.6	21.4
Be	3.75	2.77	7.48	2.03	2.77	2.28	2.68	2.55	2.04	3.16	2.53	2.38
Sc	9.70	7.92	15.1	8.57	8.74	9.15	8.77	8.85	9.08	9.66	8.41	8.40
V	68.9	69.7	65.8	54.7	63.3	57.1	60.7	60.8	70.4	63.2	66.8	71.7
Cr	16.2	13.6	56.0	17.5	12.9	12.5	10.6	9.61	10.7	10.4	13.2	15.7
Co	32.6	18.2	75.6	29.1	38.7	18.7	24.0	25.7	30.7	50.8	38.0	61.9
Ni	9.42	6.81	9.13	10.2	6.85	6.99	5.37	6.20	7.14	8.02	6.05	7.71
Cu	8.09	7.12	28.8	9.38	18.9	12.7	11.3	13.9	15.6	12.4	10.7	9.49
Zn	117	111	118	106	115	92.0	112	121	107	116	130	121
Ga	20.6	18.7	23.3	20.5	20.0	21.1	18.6	23.7	20.5	21.5	19.6	19.6
Ge	1.54	1.45	3.38	1.48	1.67	1.57	1.51	1.50	1.47	1.45	1.65	1.66
As	7.66	856	204	74.8	5.51	4.22	4.65	54.9	0.074	68.5	26.1	206
Rb	179	163	176	162	179	182	171	183	178	168	168	172
Sr	611	617	630	505	558	526	550	545	554	539	647	634
Y	24.0	22.8	24.0	22.0	23.5	23.0	23.2	24.6	24.8	23.2	24.7	23.8
Zr	513	538	595	537	534	546	527	599	523	557	615	521
Nb	40.8	41.6	40.0	36.0	36.3	38.1	37.2	41.5	39.4	37.8	43.1	42.8
Mo	3.16	4.44	3.33	3.67	3.22	4.90	3.10	4.06	3.45	3.89	3.24	3.21
Cd	0.164	0.192	0.698	0.275	0.163	0.230	0.168	0.283	0.218	0.248	0.245	0.195
In	0.053	0.040	0.054	0.056	0.052	0.059	0.048	0.062	0.048	0.060	0.045	0.045
Sn	4.43	4.51	7.48	4.23	4.25	5.03	4.33	5.25	4.84	4.49	4.97	5.01
Sb	0.580	0.393	0.566	0.437	0.427	0.192	0.424	0.739	0.293	0.571	0.447	0.357
Cs	2.41	3.04	4.42	3.46	2.93	2.74	2.23	3.65	2.52	3.42	2.99	3.03
Ba	1633	1686	1715	1762	1646	1701	1548	1823	1630	1675	1750	1775
Hf	13.9	14.0	16.0	16.2	14.4	14.6	12.9	16.0	13.5	14.7	15.6	15.2
Ta	1.92	1.92	1.81	1.92	1.84	1.96	1.72	2.17	2.00	2.01	1.92	1.97
W	119	54.5	443	162	185	80.8	91.0	126	137	237	199	275
Tl	0.698	0.745	0.661	0.754	0.694	0.639	0.703	0.989	0.567	0.731	0.869	0.762
Pb	38.7	37.0	43.0	37.0	36.1	33.8	40.5	41.5	32.9	38.6	38.1	38.2
Bi	0.124	0.081	0.118	0.217	0.091	0.155	0.142	0.102	0.073	0.101	0.077	0.099
Th	33.4	33.1	29.9	31.4	30.6	35.7	31.7	34.0	31.8	30.1	34.7	33.4
U	4.19	4.12	3.59	3.83	3.99	4.33	4.00	3.92	4.17	3.85	4.13	3.97
La	129	132	146	142	135	140	129	156	132	142	145	146
Ce	223	246	271	176	222	258	235	272	224	256	247	256
Pr	25.4	26.3	27.1	26.1	26.5	26.3	24.6	29.6	25.5	27.9	28.4	28.2
Nd	91.4	93.7	93.3	94.0	92.7	88.3	87.5	103	88.9	96.6	99.9	102
Sm	13.8	13.7	12.4	14.1	13.9	13.0	13.8	15.1	14.1	14.3	15.0	15.2
Eu	2.57	2.76	3.00	3.05	2.55	2.77	2.39	2.98	2.66	2.76	2.83	2.83
Gd	9.66	10.0	9.87	11.3	10.1	10.5	9.68	11.2	10.5	10.3	10.8	10.6
Tb	1.09	1.13	1.10	1.29	1.18	1.21	1.13	1.28	1.23	1.21	1.28	1.20
Dy	5.33	5.02	5.33	5.44	5.19	5.71	4.95	5.56	5.43	5.45	5.29	5.55
Ho	0.835	0.798	0.904	0.812	0.811	0.885	0.846	0.842	0.832	0.832	0.860	0.882
Er	2.19	1.99	2.19	2.13	2.06	2.14	2.03	2.22	2.20	2.04	2.12	2.16
Tm	0.268	0.229	0.193	0.217	0.251	0.234	0.238	0.241	0.240	0.248	0.244	0.246
Yb	1.69	1.46	1.84	1.49	1.57	1.49	1.41	1.52	1.58	1.47	1.61	1.44
Lu	0.232	0.190	0.137	0.176	0.220	0.211	0.200	0.203	0.204	0.197	0.212	0.198

Table continues

Table 1. *Continued*

Sample:	P25H	P7H	P24H4	P1H3	P25H5	P2H8	P3H10	P3H16	P6H	P2H12	P3H3	P2H11
Rock:	Dacite	Dacite	Dacite	Dacite	Dacite	Dacite	Dacite	Dacite	Dacite	Dacite	Dacite	Dacite
SiO_2	63.47	63.48	63.50	63.51	63.65	63.78	63.92	63.95	64.21	64.40	64.59	65.70
TiO_2	1.32	1.25	1.40	1.15	1.35	1.25	1.27	2.55	1.40	1.22	1.35	1.23
Al_2O_3	17.06	15.75	15.31	15.81	15.53	16.4	15.31	14.87	15.09	15.87	16.18	15.09
Fe_2O_3	1.70	1.60	2.10	1.50	2.20	1.50	1.45	1.50	1.60	1.30	1.25	1.30
FeO	2.80	3.60	3.10	3.40	3.00	3.40	3.35	3.30	3.40	3.40	3.05	3.00
MnO	0.16	0.04	0.09	0.08	0.11	0.15	0.05	0.05	0.02	0.10	0.03	0.05
MgO	1.44	1.58	1.52	1.61	1.68	1.67	1.55	1.78	1.50	1.53	1.49	1.62
CaO	3.06	3.59	3.22	2.93	3.25	2.63	2.81	3.96	3.66	2.42	2.33	2.77
Na_2O	3.60	3.40	3.60	3.60	3.20	3.30	3.40	2.40	3.40	3.31	3.30	3.30
K_2O	3.70	3.50	3.90	3.50	3.71	3.30	3.70	2.50	3.50	3.40	3.60	3.40
P_2O_5	0.57	0.80	0.77	0.83	0.87	0.77	0.70	0.80	0.77	0.80	0.77	0.83
LOI	1.00	0.85	1.23	1.40	1.09	1.15	1.98	1.79	0.95	1.77	1.54	1.02
Total	99.88	99.44	99.74	99.32	99.64	99.30	99.49	99.45	99.50	99.52	99.48	99.31
$Mg^{\#}$	0.390	0.379	0.369	0.398	0.391	0.406	0.395	0.422	0.376	0.396	0.412	0.432
Li	22.3	21.9	22.3	21.1	22.2	19.7	23.0	21.0	21.1	24.8	21.1	21.0
Be	3.28	3.20	3.19	2.50	2.69	2.48	2.62	3.43	3.26	2.71	2.67	2.22
Sc	9.45	9.19	7.99	9.56	9.80	9.34	8.71	11.0	8.95	9.25	8.37	8.65
V	66.3	71.9	64.4	59.4	71.2	60.8	66.7	72.4	68.7	64.0	60.6	60.3
Cr	18.0	10.1	40.1	15.3	17.5	14.8	10.9	28.5	10.8	19.0	11.3	10.8
Co	101	23.4	45.7	39.2	45.0	35.2	40.6	36.5	22.2	86.2	40.1	32.0
Ni	7.90	5.71	21.2	6.26	9.66	9.45	5.14	15.4	5.10	6.47	5.39	6.31
Cu	11.4	4.54	5.99	12.5	13.3	17.1	8.89	10.7	4.22	18.2	6.81	13.8
Zn	141	116	127	101	138	97.2	121	121	111	119	108	108
Ga	20.5	19.1	18.6	21.6	19.3	19.7	18.6	20.0	19.4	20.7	19.2	20.6
Ge	1.54	1.66	1.59	1.59	1.66	1.32	1.56	1.66	1.40	1.77	1.40	1.55
As	25.3	3.15	47.0	3.76	39.7	2.32	5.00	4.23	3.53	4.55	1.70	3.68
Rb	174	171	164	181	171	187	181	167	170	171	177	180
Sr	658	573	576	527	567	550	582	567	558	530	556	499
Y	21.7	23.9	23.8	23.2	24.7	24.1	24.2	38.0	23.4	23.4	23.2	23.1
Zr	531	520	490	544	606	553	561	534	522	534	524	519
Nb	42.6	39.7	41.0	38.3	43.8	38.3	37.1	41.5	38.3	38.6	37.2	35.8
Mo	3.06	3.05	4.85	3.78	3.58	3.70	3.58	3.23	2.97	3.36	3.60	3.17
Cd	0.207	0.191	0.198	0.180	0.249	0.256	0.254	0.194	0.174	0.221	0.189	0.166
In	0.051	0.051	0.050	0.046	0.051	0.054	0.054	0.042	0.045	0.049	0.046	0.046
Sn	5.03	4.03	4.91	4.06	4.68	5.71	5.18	3.50	4.31	5.37	4.16	4.18
Sb	0.631	0.216	0.498	0.354	0.588	0.536	0.572	0.590	0.255	0.294	0.289	0.471
Cs	3.31	1.91	2.98	3.13	6.44	3.07	3.06	2.28	2.16	3.05	3.00	3.13
Ba	1843	1513	1632	1696	1781	1609	1653	1571	1525	1609	1631	1584
Hf	16.8	12.8	14.5	15.6	15.7	15.2	14.4	13.2	12.9	14.7	12.9	14.0
Ta	2.16	1.86	1.90	2.05	2.13	2.05	1.89	2.03	1.76	1.93	1.78	1.82
W	370	68.3	258	241	208	225	202	138	77.0	362	193	181
Tl	0.726	0.721	0.774	0.751	1.28	0.762	0.714	0.534	0.703	0.742	0.77	0.683
Pb	40.1	35.9	35.2	37.3	36.9	38.4	38.1	36.4	36.8	37.8	37.0	38.1
Bi	0.174	0.085	0.075	0.095	0.109	0.103	0.098	0.039	0.073	0.080	0.091	0.094
Th	33.7	34.7	34.8	31.9	33.2	31.6	31.4	37.1	34.7	32.4	30.7	30.8
U	4.04	4.18	3.83	4.03	3.97	4.03	4.02	4.60	4.08	4.17	3.76	4.03
La	139	128	142	142	150	142	140	133	127	135	130	135
Ce	253	233	252	141	261	238	239	248	228	231	198	214
Pr	26.5	25.3	27.7	26.0	29.2	25.5	26.6	26.5	24.9	26.3	24.8	26.4
Nd	96.3	92.2	96.3	89.4	102	88.9	94.6	97.0	90.4	93.0	88.6	91.8
Sm	13.2	13.8	14.4	13.2	14.7	13.2	13.4	13.9	13.6	13.9	13.5	13.5
Eu	2.69	2.53	2.70	2.76	2.73	2.90	2.58	2.52	2.42	2.57	2.54	2.66
Gd	9.94	9.56	10.3	10.8	10.5	10.6	10.2	10.8	9.75	10.1	10.0	9.94
Tb	1.14	1.13	1.18	1.20	1.20	1.12	1.22	1.46	1.14	1.17	1.14	1.16
Dy	4.93	5.36	5.19	5.01	5.66	5.01	5.57	7.58	5.05	5.14	5.20	4.99
Ho	0.778	0.802	0.833	0.859	0.878	0.79	0.849	1.45	0.804	0.822	0.797	0.815
Er	1.87	2.21	2.06	2.06	2.16	2.11	2.23	3.94	2.12	2.14	2.12	2.11
Tm	0.222	0.262	0.240	0.237	0.252	0.233	0.361	0.549	0.225	0.251	0.254	0.229
Yb	1.43	1.67	1.38	1.64	1.63	1.47	1.57	3.50	1.63	1.49	1.43	1.41
Lu	0.202	0.235	0.192	0.210	0.217	0.202	0.234	0.531	0.199	0.214	0.226	0.205

[1]Mg# is the molecular proportion of MgO/(MgO + FeO), assuming 90% of total iron as ferrous iron.

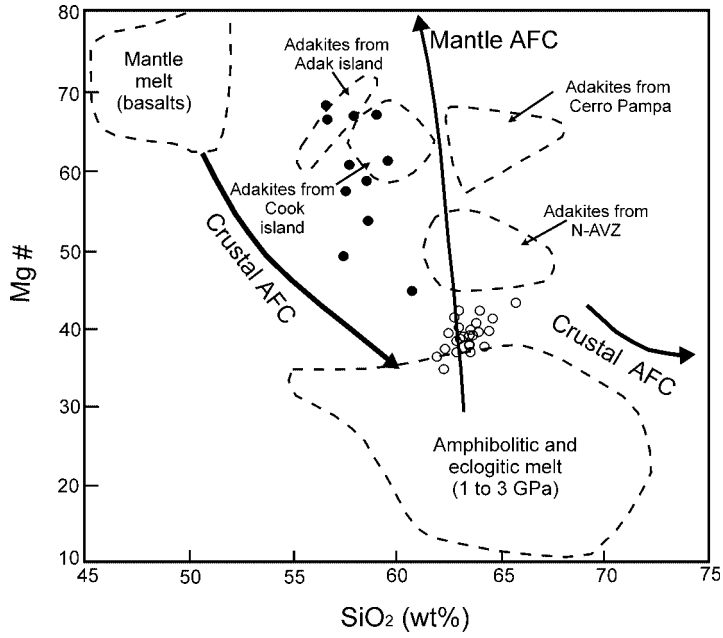

FIG. 5. Mg#–SiO_2 diagram for andesite (solid circles) and dacite (open circles) from the Zhentouya area, Hoh Xil region. The original diagram is after Stern and Kilian (1996).

analytical samples from the studied area are mainly classified into two groups, dacite and andesite (with a small amount of trachyandesite).

SiO_2 is the most abundant constituent in the andesite (56.59 to 60.74%, average 58.21%), followed by Al_2O_3 (13.78 to 17.66%, average 15.37%); MgO content is less than 6.10%, varying from 2.01 to 6.10% (average 3.97%); Na_2O > 2.50% (2.50 to 3.90%, average 3.03%). The Na_2O/K_2O ratio ranges from 0.58 to 1.39 (average 0.96). In the $Mg^{\#}$ – SiO_2 diagram (Fig. 5), andesite samples from the Zhentouya area were plotted very close to the adakites from the Adak and Cook islands, and the N-AVZ (Defant et al., 2002). Therefore, the chemical composition of these rocks is principally comparable to that of the typical adakite; they are most probably related to an adakitic melt-generation process from eclogitic lower crust (Defant et al., 2002).

The dacite exhibits SiO_2 > 61% (61.91 to 65.70%, average 63.38%), Al_2O_3 > 14% (14.87 to 17.28%, average 15.99%), MgO < 2% (1.26 to 1.82%, average 1.57%), Na_2O > 2.40% (2.40 to 4.00%, average 3.40%) , Na_2O/K_2O = 0.86 to 1.18 (average 0.95). In the $Mg^{\#}$–SiO_2 diagram (Fig. 5), dacite samples plot between the adakites from N-AVZ and amphibolitic + eclogitic melt (Defant et al., 2002).

$Mg^{\#}$ is lower in dacites (0.347 to 0.432) than in the andesites (0.449 to 0.685). The oxide variation diagrams for SiO_2, TiO_2, Al_2O_3, Fe_2O_3, FeO, MgO, CaO, Na_2O, K_2O, and P_2O_5 versus $Mg^{\#}$ are shown in Figure 6. The majority of the dacite samples show a trend of approximately constant SiO_2, TiO_2, Al_2O_3, MgO, and P_2O_5, and slightly decreasing CaO, Fe_2O_3, and K_2O, over a $Mg^{\#}$ of 0.3 to 0.5. The andesite is relatively higher in $Mg^{\#}$, and a positive correlation between $Mg^{\#}$, MgO, and CaO can be seen in Figure 6. Andesite defines a trend of slightly increasing K_2O and Fe_2O_3 over a $Mg^{\#}$ of 0.5 to 0.7, exhibiting a compositional trend that is different from that of the dacite assemblage. That is to say, the dacite does not exactly plot on the continuation from andesite on the oxide variation diagrams, especially on the $Mg^{\#}$ versus K_2O, Fe_2O_3, and CaO plots. Accordingly, dacite and andesite from the studied area probably have different genetic processes and are less likely the result of fractional crystallization from a comagmatic system.

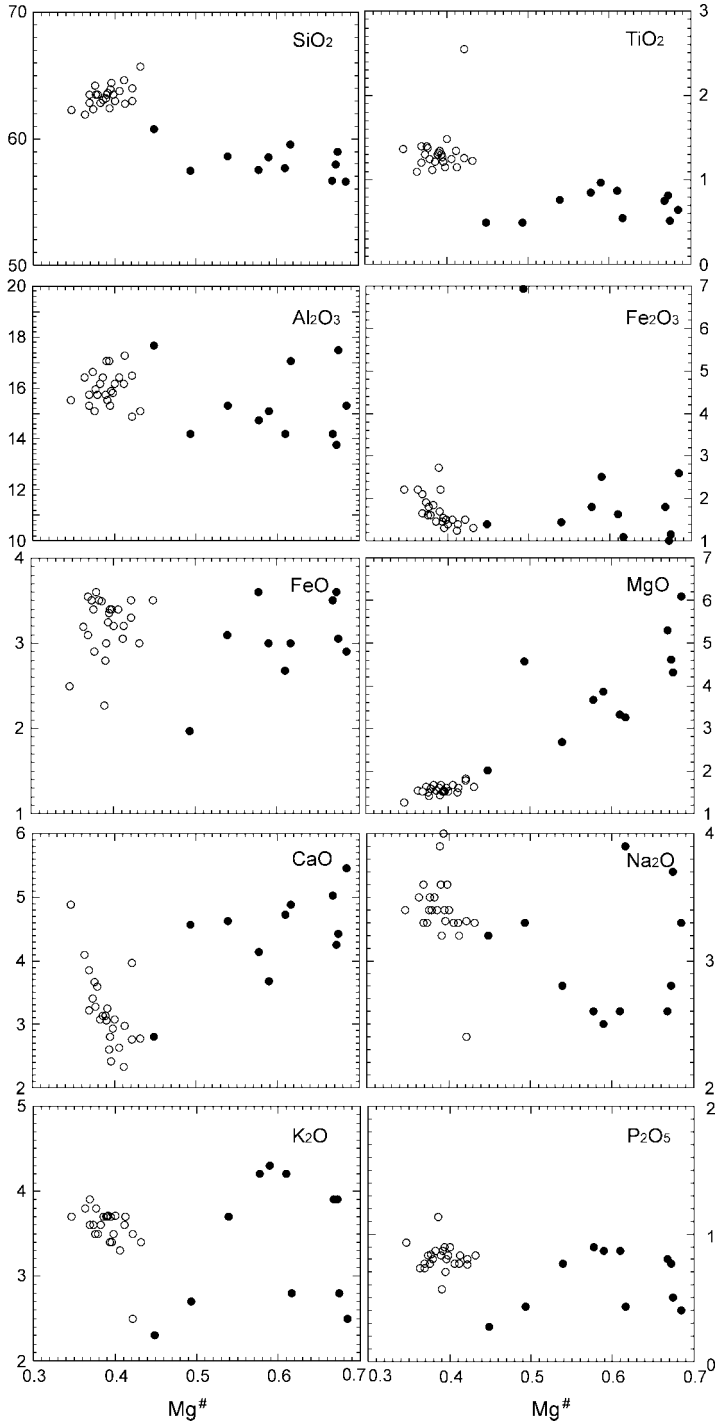

FIG. 6. Mg# versus major-element variation diagrams for andesite (solid circles) and dacite (open circles) from the Zhentouya area, Hoh Xil region.

Trace- and Rare-Earth-Element Geochemistry

Figure 7 shows the variation of trace elements as a function of $Mg^{\#}$ values, which serves as a rough index of magmatic differentiation. In the andesite from the studied area, a positive correlation between $Mg^{\#}$ and Ni, Cr, and Sc is evident. The andesite shows geochemical characteristics of high Sr and Sr/Y and slightly low Y and heavy rare earth elements (HREE), exhibiting Sr > 1000 ppm (1165 to 1653 ppm, average 1465 ppm), Y < 24 ppm (13.9 to 23.1 ppm, average 18.9 ppm), Yb < 2.00 ppm (1.08 to 1.95 ppm, average 1.55 ppm), Sr/Y > 50 (51 to 119, average 80.5), La/Yb > 28 (28 to 65, average 46). In the Sr/Yb versus Yb diagram (Fig. 8), andesite samples plot within the typical adakite field. The chemical compositions of the rocks are very close to that of typical adakites from N-AVZ (Yogodzinski et al., 1995; Stern and Kilian, 1996).

It is clear that the Ni and Cr contents are much lower in the dacite. On the $Mg^{\#}$ versus trace-element variation diagrams (Fig. 7), andesite and dacite are obviously different from each other, showing different trends on $Mg^{\#}$ versus Nb, Zr, Th, Ce and Nd, and different compositional trends as well. Compared with andesite, the dacite shows a relatively lower Sr (<660 ppm, 499 to 658 ppm, average 569 ppm), Y (>20 ppm, 21.7 to 38.0 ppm , average 24 ppm), Yb (<3.5 ppm, 1.38 to 3.50 ppm, average 1.62 ppm), Sr/Y (<30, 15 to 30, average 24), La/Yb > 38 and variable (38 to 103, average 88).

In primary mantle-normalized trace-element spider diagrams, andesite plots (Fig. 9A) show a right sloping pattern. All samples display a strong depletion in some high-field-strength elements (Nb, Ta, and Ti) compared to the primary mantle. On the other hand, some strongly incompatible elements such as Ba, Th, U, K, and Sr are strongly enriched in the andesite. Plots of the dacite from the studied area (Figs. 9B and 9C) also show a right-sloping pattern. The depletion of Nb, Ta, and Ti is clear even though the Nb, Ta depleting degree is slightly lower than that of the andesite. A striking difference between andesite and dacite is that Sr is relatively rich in the former but depleted in the latter. It is an important geochemical signature because it indicates that the plagioclase must have broken down in the andesitic magma source at the temperature and pressure of melting. On the contrary, the depletion of Sr in the dacite implies that the plagioclase is still stable in the dacitic magma source region at the pressure and temperature of partial melting. Therefore, dacite and andesite from the studied area should have different genetic processes and ahve been generated from different depths of the Tibetan Plateau crust.

The andesite from the studied area shows $(La/Yb)_N$ = 20.46–D46.36 (average 33.01), $(Ce/Yb)_N$ = 15.49–D33.98 (average 24.86), and δEu = 0.72–D0.84 (average 0.78). The dacite shows $(La/Yb)_N$ = 27.32–D74.12 (average 63.47), $(Ce/Yb)_N$ = 19.68–D50.83 (average 41.56), δEu = 0.60–0.79 (average 0.66).

According to chondrite-normalized REE distributions (Figs. 9D–9F), all the patterns for andesite and dacite are similar to one another. It indicates that both andesite and the dacite are rich in light-rare-earth elements (LREE). Moreover, the andesite exhibits a slight depletion in Eu ($\delta Eu > 0.70$), similar to typical adakites (Drummond and Defant, 1990), whereas the dacite exhibits a low to intermediate degree Eu depletion.

Sr-Nd-Pb Isotopic Systematics

Four samples of dacite from the studied area were analyzed for their Sr, Nd, and Pb isotopic ratios (Table 2). The isotopic compositions exhibit high radiogenic Sr, $^{87}Sr/^{86}Sr$ is 0.709227 to 0.709578 (average 0.7094457), and ε_{Sr} is +146.45 to +151.48 (average 149.58). However, their Nd isotopic ratio is slightly low. $^{143}Nd/^{144}Nd$ is 0.512287 to 0.512591 (average 0.512390); ε_{Nd} is negative (between –0.92 to –6.85, average –4.84).

According to the $^{143}Nd/^{144}Nd$ versus $^{87}Sr/^{86}Sr$ diagram (Fig. 10), the Sr-Nd isotopic composition of the dacite, to some degree, is similar to that of the Cordillera Blanca Batholith which was derived from newly underplated basaltic crust (Petford and Atherton, 1996), but clearly different from that of subduction-related adakites (e.g., Aleutian, Cook, and Cerro Pampa adakites; Kay, 1978; Stern and Kilian, 1996; Kay et al., 1993).

The dacite shows $^{206}Pb/^{204}Pb$ = 18.7635 to 18.7970 (average 18.7781), $^{207}Pb/^{204}Pb$ = 15.6675 to 15.7063 (average 15.6860), $^{208}Pb/^{204}Pb$ = 39.1356 to 39.2622 (average 39.1974), which indicates that the Pb isotopic ratios are rather consistent in the dacite. The Pb isotope data presented in Figure 11 were superimposed upon the Zartman and Doe (1981) Pb composition diagram. In both the $^{207}Pb/^{204}Pb$ versus $^{206}Pb/^{204}Pb$ and $^{208}Pb/^{204}Pb$ versus $^{206}Pb/^{204}Pb$ diagrams, samples were plotted

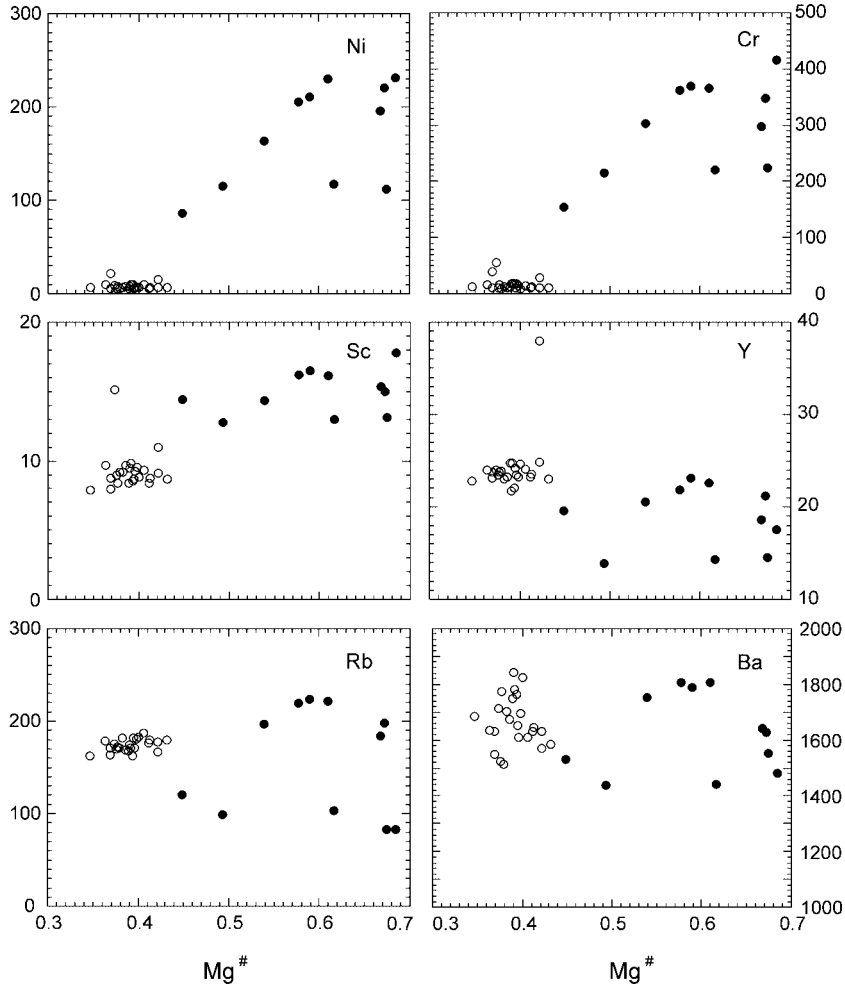

FIG. 7. Mg# versus trace-element variation diagrams for andesite (solid circles) and dacite (open circles) from the Zhentouya area, Hoh Xil region.

between or adjacent to the lower crust and upper crust. This isotopic geochemical feature suggests that the magma was derived from a source typified by crust compositions.

In addition, their Sr-Pb and Nd-Pb isotopic systematics (Fig. 12) are quite different from DMM, PREMA, MORB, HIMU, and EMI, although samples were plotted close to the region of EMII. These isotopic characteristics imply that this series of rocks could have been generated by the partial melting of continental crust, but the magma source region might be contaminated by enriched mantle material that probably provided melts that intruded the lower Tibetan Plateau crust.

Granulite Xenoliths Included in the Volcanic Rocks

Granulite xenoliths were identified mainly from the second (dacite series) eruption cycle. The granulites appear fresh in a drab red and/or greyish black color. The size generally ranges from 2 cm to 6 cm in diameter, the biggest inclusions reaching 12 cm. Massive structures (some of the xenoliths show slight gneissic textures) and medium-fine grained granoblastic textures are present. On the basis of mineral assemblage features, the granulite xenoliths can be divided into two categories, two-pyroxene granulite and clinopyroxene granulite. The former is

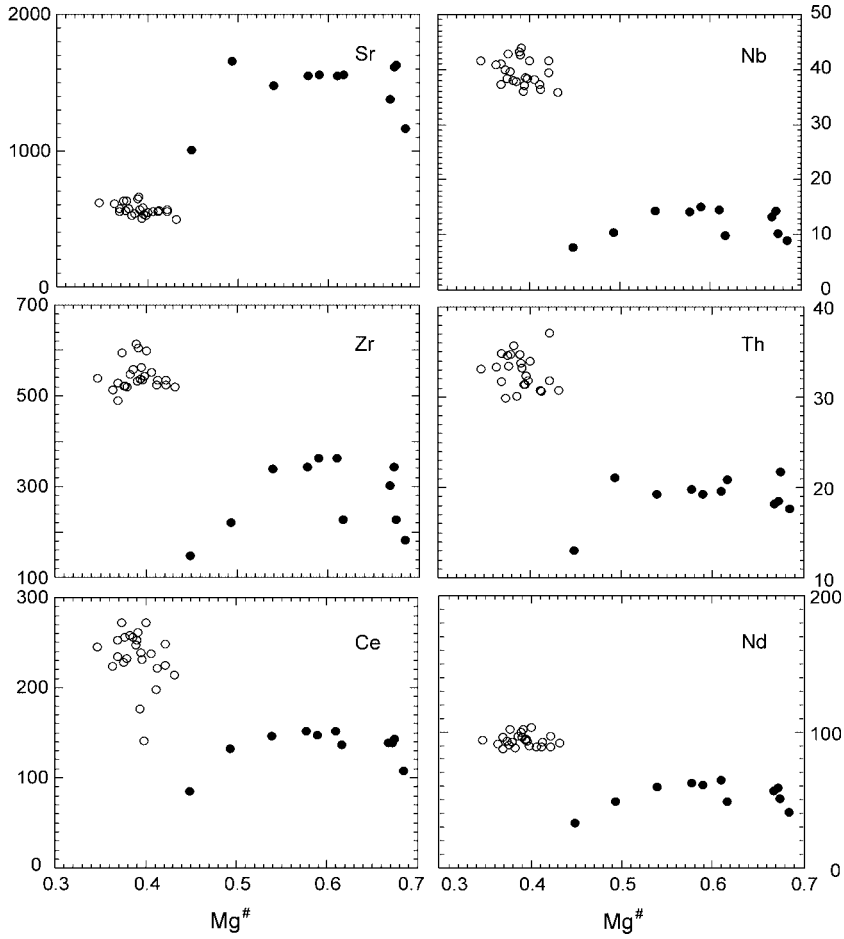

FIG. 7. *Continued*

composed of orthopyroxene, clinopyroxene, plagioclase, alkali feldspar, and biotite, and the latter consists of clinopyroxene, plagioclase, and quartz.

Two granulite xenoliths included in the dacite were studied by an electron microprobe. Results are shown in Table 3. According to the analytical data, the xenolith in Sample P26H10 is a typical two-pyroxene granulite, composed of Cpx + Opx + Pl + Af + Q. The orthopyroxene exhibits a light red color and obvious pleochroism under the microscope. Its composition is Wo (wollastonite) 1.27 to 1.34, En (enstatite) 64.92 to 66.64, and Fs (ferrosilite) 32.09 to 33.73, a typical hypersthene. The clinopyroxene is light green, with Wo 44.76, En 27.84, and Fs 27.40, and therefore assigned to salite. The biotite shows a brown-red color, reflecting Fe, Ti enrichment, Mg/(Mg+Fe*)(MF) > 0.5 (0.73 to 0.75), Ti > 0.3 (0.7700 to 0.7734), and is a titanium-ferrous biotite. The plagioclase is allotriomorphic-granular, An = 51.03–61.49, belonging to labradorite. The alkali feldspar exhibits Or = 63.62, Ab = 30.77 soda-sanidine. Based on the electron microprobe data (Table 3), the granulite was formed at a temperature between 783 and 818°C, as determined by the two-pyroxene thermometry (Wood and Banno, 1973).

The xenolith in Sample P6H belongs to the typical clinopyroxene granulite, composed of Cpx + Pl + Q. The clinopyroxene is salite, with Wo = 44.80–D44.99, En = 33.19–D33.34, Fs = 21.82–D21.86. The plagioclase An = 50.88–65.90 is labradorite.

According to the clinopyroxene-plagioclase-quartz mineral assemblage geobarometer suggested by Ellis (1980), the pressure of formation of the

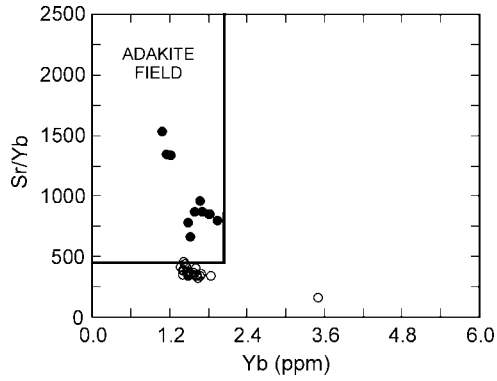

FIG. 8. Sr/Yb versus Yb diagram for andesite (solid circles) and dacite (open circles) from the Zhentouya area, Hoh Xil region. The original diagram is after Kay and Kay (2002).

clinopyroxene granulite xenolith has been calculated, as follows.

1. Plagioclase (average composition of the analysis points 11 and 12 listed in Table 3): Si^{4+}(0.9561), Ti^{4+}(0.0005), Al^{3+}(0.5110), Fe^{3+}(0.0074), Mg^{2+}(0.0026), Mn^{2+}(0.0004), Ca^{2+}(0.2026), Na^{+}(0.1360), K^{+}(0.0122). Molecular formula: $(Na_{0.367}K_{0.033})_{0.4}Ca_{0.546}Fe^{3+}_{0.02}Al_{1.378}Si_{2.578}O_8$, end member components: Ab = 38.80, An = 57.70, Or = 3.5.

2. Clinopyroxene (average composition of the analysis points 9 and 10 listed in Table 3): Si^{4+}(1.837), Ti^{4+}(0.012), $Al^{3+(IV)}$(0.163), $Al^{3+(VI)}$(0.034), Fe^{3+}(0.080), Fe^{2+}(0.346), Mg^{2+}(0.647), Mn^{2+}(0.017), Ca^{2+}(0.782), Na^{+}(0.080), K^{+}(0.000). Molecular formula: $T_{Sch16.3}(Ac+Jd)_8Hd_{36.6}Di_{39.2}$.

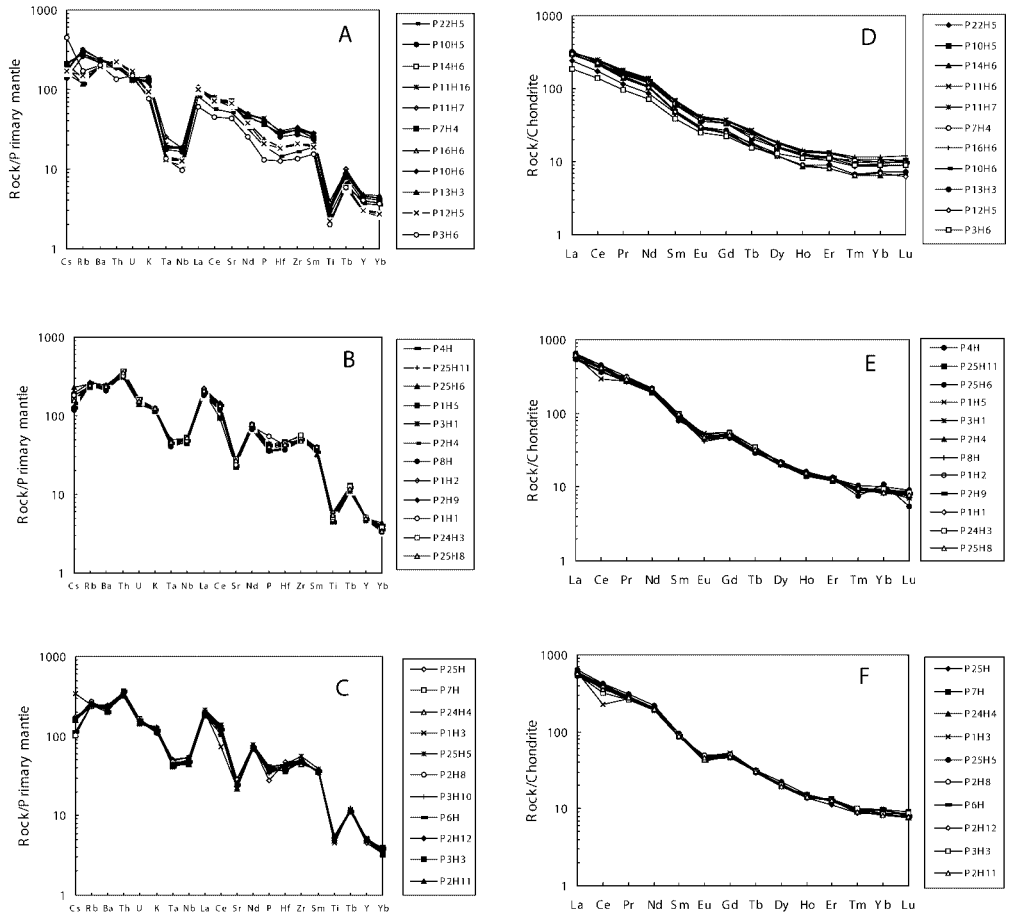

FIG. 9. Primary mantle-normalized trace element distributions and chondrite-normalized rare-earth element distributions. A. Andesite. B. Dacite. C. Dacite. D. Andesite. E. Dacite. F. Dacite. Primary mantle values are from Wood et al. (1979); chondrite values are from Sun and McDonough (1989).

TABLE 2. Sr-Nd-Pb Isotopic Data of Volcanic Rocks from the Zhentouya area, Hoh Xil region, Tibetan Plateau[1]

Sample:	P2H3	P8H	P25H8	P2H12
Rock type:	dacite	dacite	dacite	dacite
U	4.325	3.997	3.972	4.174
Th	35.744	31.727	33.397	32.387
Pb	33.76	40.465	38.185	37.75
$^{206}Pb/^{204}Pb$	18.7724 ± 10	18.7970 ± 15	18.7795 ± 8	18.7635 ± 13
$^{207}Pb/^{204}Pb$	15.6818 ± 7	15.7063 ± 10	15.6884 ± 7	15.6675 ± 10
$^{208}Pb/^{204}Pb$	39.1773 ± 19	39.2622 ± 26	39.2146 ± 18	39.1356 ± 27
Rb	158.6	168.9	164.7	159.0
Sr	757.0	557.3	696.0	526.4
$^{87}Rb/^{86}Sr$	0.6067	0.8773	0.6851	0.8744
$^{87}Sr/^{86}Sr$	0.709227 ± 14	0.709578 ± 14	0.709412 ± 14	0.709566 ± 13
ε_{Sr}	+146.45	+151.48	+149.10	+151.30
Sm	13.237	13.142	13.891	13.426
Nd	90.191	89.899	96.813	92.144
$^{147}Sm/^{144}Nd$	0.08878	0.08843	0.08679	0.08814
$^{143}Nd/^{144}Nd$	0.512287 ± 8	0.512348 ± 5	0.512591 ± 14	0.512334 ± 8
ε_{Nd}	–6.85	–5.66	–0.92	–5.93

[1]U, Th, and Pb concentrations were analyzed by ICP-MS; Sm, Nd, Rb, Sr, and isotopic ratios were measured through isotopic dilution. ε_{Nd} was calculated using $\varepsilon_{Nd} = [(^{143}Nd/^{144}Nd)_m / (^{143}Nd/^{144}Nd)_{CHUR} - 1] \times 10^4$, $(^{143}Nd/^{144}Nd)_{CHUR} = 0.512638$. ε_{Sr} was calculated using $\varepsilon_{Sr} = [(^{87}Sr/^{86}Sr)_m / (^{87}Sr/^{86}Sr)_{UR} - 1] \times 10^4$, $(^{87}Sr/^{86}Sr)_{UR} = 0.698990$. ε_{Nd} and ε_{Sr} and isotopic ratios of these rocks were not corrected for age; because this age is small, the difference between corrected and uncorrected values falls in the range of the analytical error.

3. Based on the temperature obtained from two-pyroxene granulite in Sample P26H10 determined by geothermometry, we take the equilibrium temperature of the clinopyroxene granulite as $T = 1073(K) = 800°C$. Then the ln $Kd = -2.727$ and the pressure of formation should be 0.842 GPa. According to the pressure correction method suggested by Ellis (1980), we can arrive at the corrected pressure range as follows:

P_{max}(corrected) = 0.858 GPa
(equal to a depth of 28.31 km)

P_{min}(corrected) = 0.845GPa
(equal to a depth of 27.90 km).

Discussion

Petrogenesis of the volcanic rocks

One of the critical issues in igneous petrology is regarding the generation of intermediate-silicic magmas. In general, two basic petrogenetic models have been suggested for the origin of such volcanic rocks: (1) they are fractional crystallization products of mantle-derived basaltic magma; and (2) they originated by partial melting of the lower continental crust.

Based on research done by Allergre and Minster (1978), the La/Sm-La discrimination diagram can be effectively used to identify the genesis for those volcanic rocks. As shown in Figure 13A, andesite and

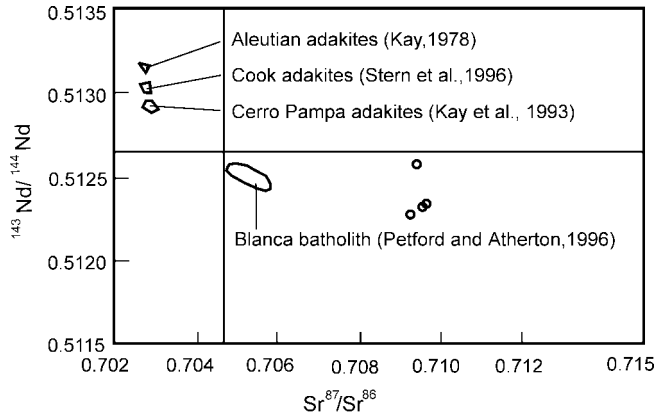

FIG. 10. $^{143}Nd/^{144}Nd$ versus $^{87}Sr/^{86}Sr$ diagram for dacite from the Zhentouya area, Hoh Xil region.

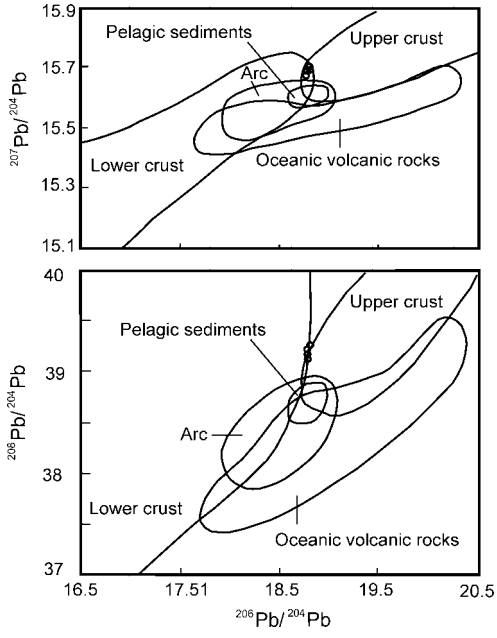

FIG. 11. Pb isotope data for dacite from Zhentouya area, Hoh Xil region. The diagram is adapted from Zartman and Doe (1981).

dacite associations from the studied area possess the lithogenesis characteristics of the source rock that underwent partial melting. The Zr/Sm-Zr diagram in Figure 13B has illustrated these characteristics.

It is well known that intermediate-silicic magmas can be generated by partial melting of the continental crust. The degree of compositional diversity among these magmas is determined by the pressure of melting, the availability of aqueous fluids, and the original composition of the protolith. Because crustal rocks are subjected to extremely high pressures and temperatures during continental collision, a contractional orogen potentially is the place where such magmas can be produced. The most dramatic effect of continental collision is that it routinely transports large volumes of supracrustal rocks to a depth of at least 60 km. Transport is accomplished by a combination of thrusting, homogeneous shortening, and subduction processes. In addition, the lithospheric mantle under a continental collision zone can be either thickened (by continued subduction) or thinned (by gravitational instability or thermal erosion), which strongly affects the heat flux into the base of the orogen. If the lithospheric mantle underlying the collisional orogen detaches and sinks, it will raise the temperature of the base of the crust to values characteristic of asthenospheric mantle (Butler et al., 1997; Patino and McCarthy, 1998), and then partial melting of the lower crust would be initiated.

A recent study conducted by Wei et al. (2001) indicated that the middle and lower crust is anomalously conductive across most of the Tibetan Plateau from south to north. The integrated conductivity of the Tibetan crust ranges from 3000 to greater than 20,000 siemens. Such pervasively high conductance suggests that partial melts and/or aqueous fluids are widespread within the Tibetan crust. In northern Tibet, the conductive layer, formed due to partial melting, is situated at a depth of 30 to 40 km (Wei et al., 2001).

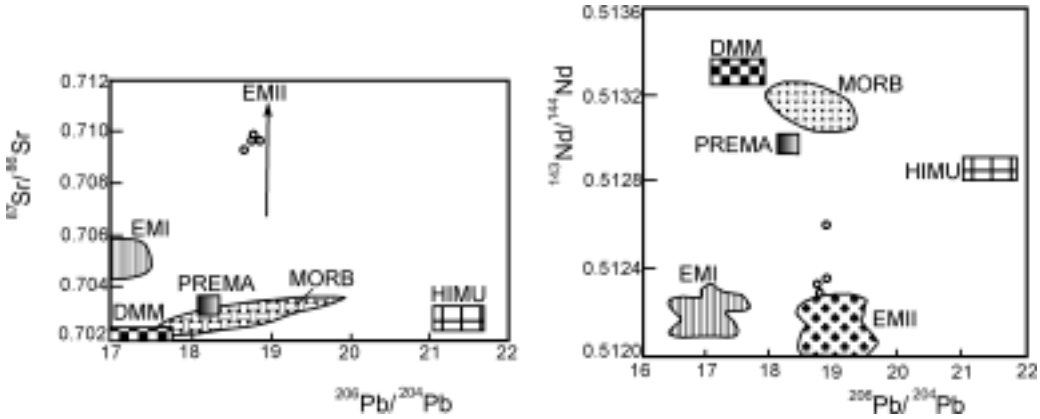

FIG. 12. $^{87}Sr/^{86}Sr$ versus $^{206}Pb/^{204}Pb$ and $^{143}Nd/^{144}Nd$ versus $^{206}Pb/^{204}Pb$ diagrams for dacite from the Zhentouya area, Hoh Xil region. Abbreviations; DMM = depleted mantle; PREMA = primary mantle; EMI = enriched mantle (type I); EMII = enriched mantle (Type II); HIMU = anomalously high $^{238}U/^{204}Pb$ mantle. The diagram is adapted from Zindler and Hart (1986).

Atherton and Petford (1993) proposed that melting of the lower crust occurs when basaltic melts underplate the lower crust; another model suggests that in areas where the continental crust is thick, the lower crust can become garnet-granulitic to eclogitic, separate from the upper crust, and sink into the mantle (Kay et al., 1993, 1994). This delamination process would bring deeply buried sections of the lower crust or the upper part of the delaminated lower crust in contact with a relatively hot mantle, which could initiate melting, and in turn bring about the formation of intermediate-silicic crust-derived volcanic rocks. Thus andesite and dacite associations from the studied area could have originated from the lower part of the thickened crust of the Tibetan Plateau.

Source regions of the andesite and dacite magmas

As shown in Figure 13, it is clear that the andesite and dacite samples from the studied area have different La/Sm and Zr/Sm ratios, and plot along two different equilibrium partial melting compositional evolutionary trend lines. In addition, on the $Mg^{\#}$ versus Sr, Nb, Zr, Th, Ce, and Nd diagrams (Fig.7), the andesite and dacite smples define contrasting trends, representing two different compositional evolution models. It suggests that the dacite and andesite probably were subjected to different genetic processes and are unlikely to be the result of fractional crystallization from a comagmatic system.

It is noteworthy that the dacite exhibits a relatively lower Sr (Sr < 660 ppm) compared with andesite (Figs. 9B and 9C). This may imply that plagioclase was stable in the dacitic magma source region at the pressure and temperature of partial melting (Rapp et al., 1999, 2002; Rapp, 2001). As mentioned above, the granulite xenoliths included in the dacite indicate a formation pressure of about 0.845 to 0.858 GPa, equal to a depth of about 27 to 30 km. At this depth (< 30 km), plagioclase is still stable. Therefore, the dacitic magma probably was generated by partial melting of the thickened Tibetan Plateau crust at a depth of about 30 km. Its source region was attended by granulite-facies PT conditions.

In contrast, the andesite from the studied area exhibits high Sr (Sr>1000 ppm) (Fig. 9A). Additionally, the andesite exhibits Y < 24 ppm, Yb < 2.00 ppm, Sr/Y > 50, located in the adakite region on the Sr/Yb-Yb diagram (Fig. 8). These facts imply that the plagioclase must have been broken down in the andesitic magma source region at the pressure and temperature of partial melting. The andesitic magma source region was attended by eclogitic-facies PT conditions. Thus, generation depth of the andesitic magma was deeper than that of the dacitic magma.

Experimental petrology and phase equilibrium research (Huang and Wyllie, 1986; Deng et al., 1996; Patino and McCarthy, 1998) indicate that when the pressure is $\leq$ 1 GPa, the liquidus line mineral of the andesitic magma system is plagioclase ± pyroxene; when > 1 GPa , it is pyroxene ± garnet ± amphibole. In cases where the buried depth is more than 45 km, continental crust will be transformed

TABLE 3. Electron Microprobe Mineral Analysis for Granulites from Cenozoic volcanic rocks, Hoh Xil region, wt%[1]

Sample:	P26H10	P26H10	P26H10	P26H10	P26H10	P26H10	P26H10	P26H10	P6H	P6H	P6H	P6H	P6H
Point:	1	2	3	4	5	6	7	8	9	10	11	12	13
Mineral:	Cpx	Opx	Opx	Pl	Pl	Af	Bi	Bi	Cpx	Cpx	Pl	Pl	Q
SiO_2	51.20	49.26	51.30	54.26	54.91	64.82	36.51	35.33	47.63	48.15	57.87	57.04	99.53
TiO_2	0.15	0.11	0.11	0.00	0.04	0.19	7.11	7.09	0.42	0.38	0.00	0.08	0.00
Al_2O_3	1.01	2.30	2.81	30.61	29.45	19.24	15.56	16.50	4.12	4.59	26.01	26.09	0.03
Cr_2O_3	0.03	0.08	0.00	0.00	0.00	0.05	0.00	0.00	0.03	0.00	0.00	0.00	0.18
FeO	16.40	21.64	21.55	0.27	0.13	0.88	10.50	11.47	13.31	13.23	0.51	0.55	0.00
MnO	0.70	0.80	0.94	0.00	0.01	0.00	0.06	0.16	0.51	0.56	0.00	0.05	0.06
MgO	9.35	25.22	23.27	0.14	0.09	0.14	17.32	17.40	11.36	11.32	0.13	0.08	0.19
CaO	20.91	0.67	0.67	11.61	10.89	1.13	0.06	0.00	21.42	21.16	11.93	10.79	0.00
Na_2O	0.45	0.07	0.04	2.89	3.19	3.42	0.46	0.44	1.17	1.00	3.09	5.34	0.00
K_2O	0.00	0.00	0.00	0.76	0.88	10.75	8.97	8.98	0.00	0.00	0.49	0.66	0.02
NiO	0.00	0.02	0.00	0.07	0.18	0.00	0.00	0.03	0.06	0.00	0.01	0.00	0.00
Total	100.20	100.17	100.68	100.61	99.79	100.63	96.55	97.40	100.04	100.38	100.04	100.68	100.01
[O]=	6	6	6	8	8	8	22	22	6	6	8	8	2
Si	1.9752	1.8471	1.9001	2.4270	2.4726	2.9409	5.2808	5.1023	1.8338	1.8397	2.5945	2.5621	0.9969
Al	0.0459	0.1016	0.1227	1.6137	1.5630	1.0288	2.6526	2.8085	0.1870	0.2067	1.3744	1.3812	0.0004
Ti	0.0044	0.0031	0.0031	0.0000	0.0014	0.0065	0.7734	0.7700	0.0122	0.0109	0.0000	0.0027	0.0000
Cr	0.0009	0.0024	0.0000	0.0000	0.0000	0.0018	0.0000	0.0000	0.0009	0.0000	0.0000	0.0000	0.0014
Fe	0.5291	0.6787	0.6675	0.0101	0.0049	0.0334	1.2701	1.3853	0.4286	0.4227	0.0191	0.0207	0.0000
Mn	0.0229	0.0254	0.0295	0.0000	0.0004	0.0000	0.0074	0.0196	0.0166	0.0181	0.0000	0.0019	0.0005
Mg	0.5376	1.4095	1.2847	0.0093	0.0060	0.0095	3.7340	3.7455	0.6519	0.6447	0.0087	0.0054	0.0028
Ca	0.8643	0.0269	0.0266	0.5564	0.5254	0.0549	0.0093	0.0000	0.8836	0.8662	0.5731	0.5193	0.0000
Na	0.0337	0.0051	0.0029	0.2506	0.2785	0.3009	0.1290	0.1232	0.0873	0.0741	0.2686	0.4651	0.0000
K	0.0000	0.0000	0.0000	0.0434	0.0506	0.6222	1.6551	1.6544	0.0000	0.0000	0.0280	0.0378	0.0003
Ni	0.0000	0.0006	0.0000	0.0025	0.0065	0.0000	0.0000	0.0035	0.0019	0.0000	0.0004	0.0000	0.0000
Sum	4.0139	4.1004	4.0370	4.9131	4.9092	4.9988	15.512	15.612	4.1038	4.0831	4.8667	4.9961	1.0023
Wo	44.76	1.27	1.34						44.99	44.80			
En	27.84	66.64	64.92						33.19	33.34			
Fs	27.40	32.09	33.73						21.82	21.86			
An				51.03	61.49	5.61					65.90	50.80	
Ab				29.47	32.59	30.77					30.88	45.50	
Or				5.10	5.92	63.62					3.20	3.70	
Ca							1.86	0.00					
Mg							74.48	73.00					
Fe							25.33	27.00					

[1]Analyzed by Electron Microprobe Section, Xi'an Institute of Geology and Mineral Resources, 2001.

into eclogite (Yardley and Valley, 1997). The andesitic magma system that was generated from the lower part of the thickened crust of the Tibetan Plateau would not be in equilibrium with plagioclase during the partial melting process and differentiation, and was evidently generated from an eclogitic source at a depth of at least 45 km.

Volcanic melt generation model

Mantle-derived alkaline volcanic rocks have erupted on the Tibetan Plateau since at least 45 million years ago. The shoshonitic to ultrapotassic volcanic rock series is the most widespread and common type in northern Qiangtang and the Hoh Xil areas (Liu, 1998; Ugo, 1990; Arnaud et al., 1992; Turner et al., 1996; Deng, 1998; Chi et al., 1999; Deng and Sun, 1999; Lai, 1999; Miller et al., 1999; Wang, 1999; Yang et al., 1999). The generation of andesitic and dacitic magmas in the thickened crust of the Tibetan Plateau requires addition of heat that was probably provided by mantle-derived melts intruded into the crust. In fact, the isotopic characteristics of the dacite from the studied area imply that this series was generated by crust partial

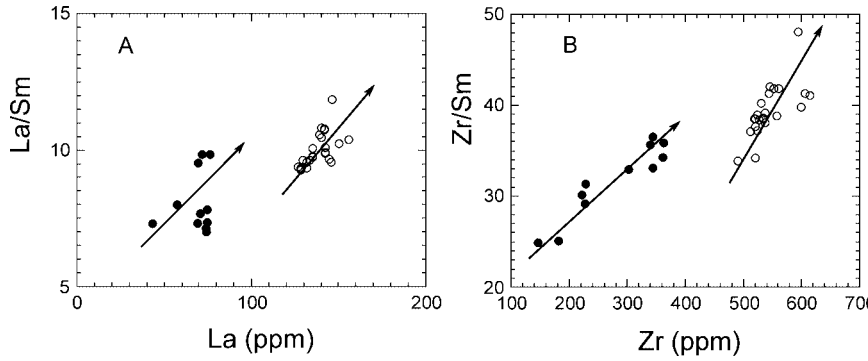

FIG. 13. La-La/Sm (A) and Zr-Zr/Sm (B) diagrams for andesite (solid circles) and dacite (open circles) from the Zhentouya area, Hoh Xil region.

melting. But the magma source region might have been contaminated by mantle-derived melts intruded into the thickened lower crust. Therefore, mantle-derived alkaline magma may have provided extra heat for the thickened Tibetan crust.

As we know, when basaltic magmas are emplaced into the continental crust, the melting and generation of intermediate-silicic magma can be expected (Herbert and Sparks, 1988). Convincing evidence exists that most of the large granite complexes in the continental crust are the result of crustal anatexis (Pitcher, 1987). There is also widespread evidence that basaltic magma from the mantle in many cases is intimately associated with the generation of intermediate-silicic magmas (Hildreth, 1981). Petrological and geochemical features of many intermediate-silicic igneous rocks are also convincingly explained by admixture of a mantle-derived (mafic) component with a crustal melt. According to experimental studies (Herbert and Sparks, 1988), basalt intruded into the crust causes melting and high heat flow. Indeed, the basalt underplating of the crust is currently a popular idea to explain both large-scale crustal melting and the strongly layered character of the lower crust. The Tibetan thickened crust is strongly layered in terms of its composition, density, and mechanical behavior (Molnar, 1988). The upper crust is relatively cold and brittle, whereas the middle-lower crust is hotter (Wei et al., 2001), has a higher density, deforms in a ductile manner, and is characterized by prominent horizontal layering. Basalt magma is emplaced into the continental crust as dikes and sills. In some cases, where the rate of magma input is high, these intrusions can coalesce to form large magma chambers (Fig. 14). In general, sills provide a more promising situation in which extensive crustal melting can occur. Horizontal intrusions concentrate their heat at a particular level in the crust and do not dissipate it over a large depth range (Herbert and Sparks, 1988). A large or region of partially molten crust provides an effective density barrier. Herbert and Sparks (1988) suggested that basalt magma reaching such a level spreads out as horizontal intrusions (Fig. 14).

Inasmuch as the Qiangtang and Hoh Xil areas constitute the core of the Tibetan Plateau, the crust evidently was thickened during the Late Paleogene to Neogene (Deng, 1998). It is a typical continental collision orogenic belt. In addition, the intrusion of mantle-derived magma (shoshonitic and ultrapotassic series) and underplating in the lower crust led to partial melting of the crustal rock sequence. Therefore, the lower part of the thickened Tibetan crust, to some degree, had been favorable to generate crust-derived magmas during the Cenozoic Period. Especially, when mantle-derived alkaline magma intimately intruded the Tibetan lower crust and/or underplated the Moho, the initial melting of intermediate-silicic crust-derived magmas would be expected (Fig. 14).

At the depth of >45 km in eclogitic facies, partial melting of the thickened Tibetan crust would result in s high-Sr, low-Y andesitic magma showing a somewhat adakite-like signature. At a depth of about 30 km under granulitic-facies conditions, where plagioclase is stable, partial melting of the crust would lead to a dacitic magma that shows a strong depletion in Sr and contains many granulite xenoliths. The formation of the andesite and dacite

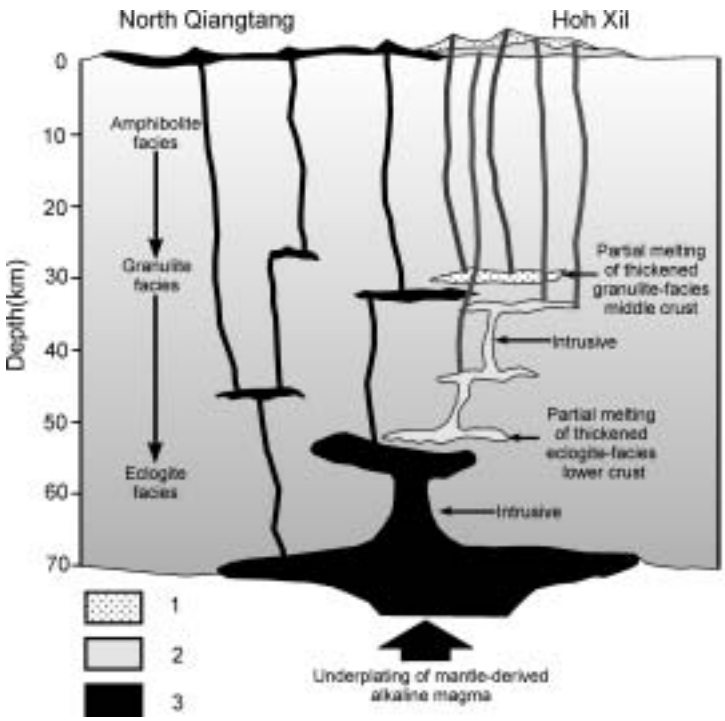

FIG. 14. Sketch model for the andesitic and dacitic magmas formation by emplacement of mantle-derived alkaline magma into thickened Tibetan crust. Legend: 1 = crust-derived dacite in the studied area; 2 = crust-derived andesite in the studied area; 3 = mantle-derived alkaline (ultrapotassic and shoshonitic series) magma.

associations developed in the studied area should be ascribed to this kind of tectonic setting. A sketch of the petrogenetic model is summarized in Figure 14.

Magma generation during continental collision requires the convergence of appropriate source rocks and requisite thermal conditions. Rocks of sedimentary and igneous origin are the most abundant in the continental crust, and can partially melt to yield intermediate-silicic magmas. Belts of continental collision thus are fertile environments for magma generation on a large scale. Whether this potential is realized or not depends on the thermal structure of the orogen. Processes such as thermal blanketing resulting from tectonic thickening, delamination of the subcrustal lithosphere, underplating of mantle-derived magma, and extensional collapse of thickened crust favor the attainment of temperature high enough to cause widespread crustal melting. Therefore, identification of the andesite and dacite associations in the Zhentouya area, Hoh Xil region constitute significant evidence and an example for further study of magma generation during continental collision.

Acknowledgments

This work was jointly supported by the National Natural Science Foundation of China (NSFC, Grant Nos. 40272042, 40072029) and the Teaching and Research Award Program for Outstanding Young Teachers in Higher Educational Institutions, Ministry of Education (MOE), China. We thank A.-L. Guo and X.-L. Zhang for assistance with English exposition.

REFERENCES

Allegre, C. J., and Minster, J. F., 1978, Quantitative method of trace element behavior in magmatic processes: Earth and Planetary Science Letters, v. 38, p. 1–25.

Argand, E., 1924, La tectonique de L' Asie: Proceedings of the 13th International Geological Congress, v. 7, p. 171–172.

Arnaud, N. O., Vidal, P., Tapponnier, P., Matte, P., and Deng, W. M., 1992, The high K_2O volcanism of northwestern Tibet: Geochemistry and tectonic implications: Earth and Planetary Science Letters, v. 111, p. 351–367.

Atherton, M. P., and Petford, N., 1993, Generation of sodium-rich magmas from newly underplated basaltic crust: Nature, v. 362, p. 144–146.

Butler, R. W. H., Harris, N. B. W., and Whittington, A. G., 1997, Interactions between deformation, magmatism, and hydrothermal activity during active crustal thickening: A field example from Nanga Parbat, Pakistan Himalayas: Mineralogical Magazine, v. 61, p. 37–68.

Chi, X. G., Li, C., Jin, W., Liu, S., and Yang, R. H., 1999, Cenozoic volcanism evolutionary and uplifting mechanism of the Qinghai-Tibet plateau: Geological Review, v. 45, p. 978–986 (in Chinese).

Coleman, M., and Hodges, K., 1995, Evidence for Tibetan plateau uplift before 14 Myr ago from a new minimum age for east-west extension: Nature, v. 374, p. 49–52.

Defant, M. J., Xu, J. F., Kepezhinskas, P., Wang, Q., Zhang, Q., and Xiao, L., 2002, Adakites: Some variations on a theme: Acta Petrologica Sinica, v. 18, p. 129–142.

Deng, J. F., Zhao, H. L., Mo, X. X., Wu, Z. X., and Luo, Z. H., 1996, Continental roots–plume tectonics of China—key to the continental dynamics: Beijing, China, Geological Publishing House, 112 p. (in Chinese).

Deng, W. M., 1998, Cenozoic intraplate volcanic rocks in the Northern Qinghai-Xizang plateau: Beijing, China, Geological Publishing House, 168 p. (in Chinese).

Deng, W. M., and Sun, H. J., 1998, Features of isotopic geochemistry and source region for the intraplate volcanic rocks from northern Qinghai-Tibet plateau: Earth Science Frontiers, v. 5, p. 307–317 (in Chinese).

_____, 1999, Cenozoic volcanism and the uplifting mechanism of the Qinghai-Tibet plateau: Geological Review, v. 45, p. 952–958 (in Chinese).

Dewey, J. F., and Burke, K., 1973, Tibetan Variscan and Precambrian basement reactivation: Products of continental collision: Journal of Geology, v. 81, p. 683–692.

Drummond, M. S., and Defant, M. J., 1990, A model for trondhjemite-tonalite-dacite genesis and crustal growth via slab melting: Journal of Geophysical Research, v. 95, p. 21,503–21,521.

Ellis, D. J., 1980, Osumilite-sapphirine-quartz granulites from Enderby Land, Antarctica: P-T conditions of metamorphosis, implications for garnet-cordierite equilibria and the evolution of the deep crust: Contributions to Mineralogy and Petrology, v. 74, p. 201–210.

England, P. C., and Houseman, G. A., 1988, The mechanics of the Tibetan plateau: Philosophical Transactions of the Royal Society of London, Series A, v. 326, p. 301–319.

_____, 1989, Extension during continental convergence, with application to the Tibetan plateau: Journal of Geophysical Research, v. 94, p. 17,561–17,579.

Herbert, E. H., and Sparks, R. S. J., 1988, The generation of granitic magmas by intrusion of basalt into continental crust: Journal of Petrology, v. 29, p. 599–624.

Hildreth, W., 1981, Gradients in silicic magma chambers: Implication for lithospheric magmatism: Journal of Geophysical Research, v. 86, p. 92–153.

Huang, W. L., and Wyllie, P. J., 1986, Phase relationships of gabbro-tonalite-granite H_2O at 15 kbar with applications to differentiation and anatexis: American Mineralogist, v. 71, p. 301–316.

Kay, R. W., 1978, Aleutian magnesian andesites: Melts from subducted Pacific Ocean crust: Journal of Volcanology and Geothermal Research, v. 4, p. 117–132.

Kay, R. W., and Kay, S. M., 2002, Andean adakites: Three ways to make them: Acta Petrologica Sinica, v. 18, p. 303–311.

Kay, S. M., Coira, B., and Viramonte, J., 1994, Young mafic back-arc volcanic rocks as guides to lithospheric delamination beneath the Argentine Puna Plateau, Central Andes: Journal of Geophysical Research, v. 99, p. 14,323–14,339.

Kay, S. M., Ramos, V. A., and Marquez, Y. M., 1993, Evidence in Cerro Pampa volcanic rocks for slab-melting prior to ridge-trench collision in southern South America: Journal of Geology, v. 101, p. 703–714.

Lai, S. C., 1999, Petrogenesis of the Cenozoic volcanic rocks from the northern part of the Qinghai-Tibet plateau: Acta Petrologica Sinica, v. 15, p. 98–104 (in Chinese).

Lai, S. C., and Liu, C. Y., 2001, Enriched upper mantle and eclogitic lower crust in north Qiangtang, Qinghai-Tibet plateau: Petrological and geochemical evidence from the Cenozoic volcanic rocks: Acta Petrologica Sinica, v. 17, p. 459–468 (in Chinese).

Lai, S. C., O'Reilly, S. Y., and Zhang, M., 2003, Geochemistry of Cenozoic adakitic rocks from Qiangtang of the Tibetan Plateau: Evidence of Partial Melting of the thickened Tibetan crust: Earth and Planetary Science Letters (submitted).

Le Bas, M. J., 1986, A chemical classification of volcanic rocks based on the total alkaline-silica diagram: Journal of Petrology, v. 27, p. 745–750.

Liu, J. Q., 1998, Volcanoes in China: Beijing, China, Science Press, 110 p. (in Chinese).

Miller, C., Schuster, R., Klotzli, U., Frank, W., and Purtscheller, F., 1999, Post-collisional potassic and ultrapotassic magmatism in SW Tibet: Geochemical and Sr, Nd, Pb, O isotopic constraints for mantle source characteristics and petrogenesis: Journal of Petrology, v. 40, p. 1399–1424.

Molnar, P., 1988, A review of geophysical constraints on the deep structure of the Tibetan Plateau, the Himalaya and the Karakoram, and their tectonic

implications: Philosophical Transactions of the Royal Society of London, Series A, v. 326, p. 33–88.

Ni, J., and Barazangi, M., 1984, Seismotectonics of the Himalayan collision zone: Geometry of the underthrusting Indian plate beneath the Himalaya: Journal of Geophysical Research, v. 89, p. 1147–1163.

Patino, D. A. E., and McCarthy, T. C., 1998, Melting of crustal rocks during continental collision and subduction: Dordrecht, Netherlands, Kluwer Academic Publishers, 55 p.

Petford, N., and Atherton, M. P., 1996, Na-rich partial melting from newly underplated basaltic crust: The Cordillera Blanca Batholith, Peru: Journal of Petrology, v. 37, p. 1491–1521.

Pitcher, W. S., 1987, Granites and yet more granites forty years on: Geologische Rundschau, v. 76, p. 51–79.

Platt, J. P., and England, P. C., 1994, Convective removal of lithosphere beneath mountain belts: Thermal and mechanical consequences: American Journal of Science, v. 294, p. 307–336.

Powell, C. M., and Conaghan, P. G., 1973, Plate tectonics and the Himalayas: Earth and Planetary Science Letters, v. 20, p. 1–12.

Qi, L., and Gregoire, D. C., 2000, Determination of trace elements in twenty six Chinese geochemistry reference materials by inductively coupled plasma-mass spectrometry: The Journal of Geostandards and Geoanalysis, v. 24, p. 51–63.

Qi, L., Hu, J., and Gregoire, D. C., 2000, Determination of trace elements in granites by inductively coupled plasma mass spectrometry: Talanta, v. 51, p. 507–513.

Rapp, R. P., 2001, A review of experimental constraints on adakite petrogenesis, *in* Symposium on adakite-like rocks and their geodynamic significance: Beijing, China, p. 10–13.

Rapp, R. P., Shimizu, N., Norman, M. D., and Applegate, G. S., 1999, Reaction between slab-derived melts and peridotite in the mantle wedge: Experimental constraints at 3.8 GPa: Chemical Geology, v. 160, p. 335–356.

Rapp, R. P., Xiao, L., and Shimizu, N., 2002, Experimental constraints on the origin of potassium-rich adakites in eastern China: Acta Petrologica Sinica, v. 18, p. 293–302.

Stern, C. R., and Kilian, R., 1996, Role of the subducted slab, mantle wedge and continental crust in the generation of adakites from the Andean Austral volcanic zone: Contributions to Mineralogy and Petrology, v. 123, p. 263–281.

Sun, S. S., and McDonough, W. F., 1989, Chemical and isotopic systematics of oceanic basalts: Implications for mantle composition and processes, *in* Saunders, A. D., and Norry, M. J., eds., Magmatism in the ocean basin: Geological Society of London Special Publication, v. 42, p. 313–345.

Turner, S., Arnaud, N., Liu, J., Rogers, N., Hawkesworth, C. J., Harris, N., Kelley, S., van Calsteren, P., and Deng, W., 1996, Post-collision, shoshonitic volcanism on the Tibetan Plateau: Implications for convective thinning of the lithosphere and the source of ocean island basalts: Journal of Petrology, v. 37, p. 45–71.

Ugo, P., 1990, Shoshonitic and ultrapotassic post-collisional dykes from northern Karakorum (Sinkiang, China): Lithos, v. 26, p. 305–316.

Wang, B. X., Ye, H. F., and Peng, Y. M., 1999, Isotopic geochemistry features and its significance of the Mesozoic–Cenozoic volcanic rocks from Qiangtang basin, Qinghai-Tibet plateau: Geological Review, v. 45, p. 946–951 (in Chinese).

Wei, W. B., Unsworth, M., Jones, A., Booker, J., Tan, H. D., Nelson, D., Chen, N. S., Li, S. H., Solon, K., Bedrosian, P., Jin, S., Deng, M., Ledo, J., Kay, D., and Roberts, B., 2001, Detection of widespread fluids in the Tibetan crust by magnetotelluric studies: Science, v. 292, p. 716–718.

Wood, B. J., and Banno, S., 1973, Garnet-orthopyroxene relationships in simple and complex systems: Contributions to Mineralogy and Petrology, v. 42, p. 109–124.

Wood, D. A., Joron, J. L., Treuil, M., Norry, M., and Tarney, J., 1979, Elemental and Sr isotope variations in basic lavas from Iceland and the surrounding sea floor: Contributions to Mineralogy and Petrology, v. 70, p. 39–319.

Wortel, M. J. R., Hansen, U., and Sabadini, R., 1992, Convective removal of thermal boundary layer of thickened continental lithosphere: A brief summary of causes and consequences with special reference to the Cenozoic tectonics of the Tibetan Plateau and surrounding regions: Tectonophysics, v. 223, p. 67–73.

Yang, D. M., Li, C., and He, Z. H., 1999, Petrochemistry and tectonic settings of the volcanic rocks of Songwori in Nima county, Tibet: Geological Review, v. 45, p. 972–977 (in Chinese).

Yardley, B. W. D., and Valley, J. W., 1997, The petrologic case for a dry lower crust: Journal of Geophysical Research, v. 102, p. 12173–12185.

Yogodzinski, G. M., Kay, R. W., Volynets, O. N., Koloskov, A. V. , and Kay, S. M., 1995, Magnesian andesite in the western Aleutian Komandorsky region: Implications for slab melting and processes in the mantle wedge: Geological Society of America Bulletin, v. 107, p. 505–519.

Zartman, R. E., and Doe, B. R., 1981, Plumbotectonics—the model: Tectonophysics, v. 75, p. 135–162.

Zhang, Y. F., and Zheng, J. K., 1994, An introduction to the geological evolution of Hoh Xil and its adjacent region, Beijing, China: Seismological Press, 86 p. (in Chinese).

Zhao, W., and Morgan, W. J., 1987, Injection of Indian crust into Tibetan lower crust: A two-dimensional finite-element model study: Tectonics, v. 6, p. 489–504.

Zindler, A., and Hart, S. R., 1986, Chemical geodynamics: Annual Review of Earth and Planetary Science, v. 14, p. 493–573.